

Mechanisms of Adsorption and Surface-mediated Aggregation of Intrinsically Disordered  
Protein Tau at Model Surfaces

By

Nicolas Mucci

Submitted to the graduate degree program in Chemical and Petroleum Engineering and the  
Graduate Faculty of the University of Kansas in partial fulfillment of the requirements for the  
degree of Master of Science.

---

Chairperson: Dr. Prajna Paramita Dhar

---

Dr. T. Christopher Gamblin

---

Dr. Stevin Gehrke

---

Dr. Kevin Leonard

Date Defended: May 13, 2015

The Thesis Committee for Nicolas Mucci  
certifies that this is the approved version of the following thesis:

Mechanisms of Adsorption and Surface-mediated Aggregation of Intrinsically Disordered  
Protein Tau at Model Surfaces

---

Chairperson Dr. Prajnaparamita Dhar

Date approved: May 13, 2015

## ACKNOWLEDGEMENTS

I would like to start by thanking my advisor, Dr. Dhar. Working with you has been a pleasure and I couldn't think of a better mentor to have for the past two years. I have learned so much during my time here and I wouldn't trade the experience for anything. Thank you for putting up with me, and helping me to grow as a researcher and an engineer.

I would next like to thank my collaborators, specifically Dr. Gamblin and Smita Paranjape. I have learned a lot talking with both of you, and you have been a great help to me and this project. Without your aid, this Thesis would not have been possible. Thank you for letting me bug you constantly for more and more proteins.

Lastly, I would like to thank my research group: Aishik, Saba, Rachel, Nabil, Lorena, Coleman, and Yan. From my basketball background I have come to think of teammates as not only my friends but my family, and that is exactly how I see y'all now. Over the past two years, our group has become like a family, and I couldn't have asked for a better one to struggle with, and grow with over that time.

Thank you all. It has been my pleasure.

# TABLE OF CONTENTS

<b>List of Figures</b>	<b>iv</b>
<b>List of Tables</b>	<b>vii</b>
<b>Abstract</b>	<b>viii</b>
<b>1. Introduction</b>	<b>1</b>
<b>2. Materials and Methods</b>	<b>12</b>
<b>3. Results and Discussion</b>	<b>18</b>
<b>3.1-Protein Adsorption to Solid Surfaces</b>	<b>18</b>
<b>3.2-Adsorption and Aggregation of Proteins on Lipid Covered Surfaces</b>	<b>31</b>
<b>4. Conclusions and Future Directions</b>	<b>39</b>
<b>5. Summary</b>	<b>41</b>
<b>REFERENCES</b>	<b>42</b>

# LIST OF FIGURES

<b>Figure 1:</b> Hallmarks of Various Neurodegenerative Diseases.....	1
<b>Figure 2:</b> Brain Volume Comparison Between Healthy and Alzheimer's Brain .....	2
<b>Figure 3:</b> Mechanism of Amyloid Beta Formation .....	3
<b>Figure 4:</b> Tau Isoforms, amino acid sequence, and Possible "Paper clip" Conformation and Hypothesized Aggregated Structure.....	4
<b>Figure 5:</b> Kyte & Doolittle plots for (a) the wild-type protein, (b) AIP, and (c) R5L. Values close to 1 mean that a region is more hydrophobic. As can be seen in the figures, the location where the mutation in the binding region occurs is one of the most hydrophobic regions in the wild-type protein. This same region in the AIP is much less hydrophobic than the wild-type. For R5L, the mutation increases the hydrophobicity of the N-terminus. ....	10
<b>Figure 6:</b> Lipid structure of DPPE, DPPS, and DOPS .....	13
<b>Figure 7:</b> (a) Maximum change in Frequency and (b) maximum calculated adsorbed mass of Htau40WT on Polystyrene as a function of protein concentration, showing a saturation in protein adsorption beyond 450nM protein concentration .....	19
<b>Figure 8:</b> (a,d) Changes in frequency (Hz) and (b,e) changes in the calculated adsorbed mass (ng/cm <sup>2</sup> ) of protein as a function of time during adsorption of 450nM Htau40WT (a,b) and AIP (d,e) on different surfaces (gold (blue), silicon dioxide (red), and polystyrene (black)). Figure 8 (c,f) represent changes in frequency due to protein desorption when buffer was run across surfaces saturated with Htau40WT (c) and AIP (f).....	20
<b>Figure 9:</b> (a,c,e) change in frequency (Hz) as a function of time and (b,d,f) change in the calculated adsorbed mass (ng/cm <sup>2</sup> ) as a function of time, during adsorption of 450nM Htau40WT (black) and AIP (red) proteins on polystyrene, gold, and silicon dioxide surfaces. The green curves show a fit to	

exponential decay curves, showing the kinetics of protein adsorption. The fitting parameters and goodness of fit are shown in Table 1. .... 23

**Figure 10:** Dissipation vs. Frequency plots of 450nM Htau40WT (black) and AIP (red) proteins on different surfaces: (a) polystyrene, (b) gold, and (c) silicon dioxide, showing that polystyrene surfaces show a difference in rigidity of the proteins, while silicon dioxide and gold surfaces do not. .... 25

**Figure 11:** (a,b,c) change in frequency (Hz) and (d,e,f) change in the calculated adsorbed mass (ng/cm<sup>2</sup>) as a function of time, during the adsorption of the fluorescent indicator Thioflavin (ThT) to surfaces saturated with Htau40WT (black) or AIP (red) proteins, or a blank surface (green). ThT has been shown to adsorb to aggregated protein forms. .... 28

**Figure 12:** AFM images of wild-type tau protein and AIP on silicon dioxide wafers and polystyrene coated wafers. Image (a) and (d) show the bare polystyrene and silicon dioxide surfaces, respectively. These images show no surface features greater than 1nm high, which can be seen in the line graph below the image, and can therefore were considered flat. (b) shows the wild-type protein on the polystyrene surface, while (c) shows the AIP on polystyrene. (e) is an image of the wild-type tau protein on the silicon dioxide surface, while (f) is an image of the AIP on silicon dioxide, and there were few smaller aggregates present. The line graphs below each image represents the height of the surface features indicated by the arrows on the image themselves. .... 30

**Figure 13:** Lipid Adsorption to a silicon dioxide surface. Here we see that DPPE:DOPS adsorbs more than DPPE:DPPS, but more importantly, based on the shape of the curves for both lipid mixtures, we believe that the lipids adsorb as vesicles .... 32

**Figure 14:** Different Proteins adsorption to a surface covered in DPPE:DPPS. Htau40WT (black) adsorbs more than R5L (red), but over time we see a loss of mass for the surface with R5L. This could possibly be due to the protein rupturing the lipid vesicle which then releases fluid and results in the mass decrease. .... 33

**Figure 15:** Different proteins adsorption to a surface covered in DPPE:DOPS. R5L (red) adsorbs more than Htau40WT (black), but over time there is a significant loss of mass for the surface with R5L. This is again most likely attributed to a disruption in the lipid vesicle. Interestingly, we see a similar trend, although not to the same extent, with the wild-type protein showing that it too has the ability to penetrate the lipid membrane. .... 34

**Figure 16:** Adsorption of Htau40WT to a surface covered in DPPE:DPPS (red) and DPPE:DOPS (black). The wild-type protein adsorbs slightly more to the DPPE:DPPS surface, but for the surface covered in DPPE:DOPS, the wild-type protein seems to have the ability to rupture the vesicle, possibly due to the DPPE:DOPS being a more fluid mixture than the DPPE:DPPS. .... 35

**Figure 17:** R5L adsorption to a surface covered in DPPE:DPPS (red) and DPPE:DOPS (black). The protein adsorbs more to the DPPE:DOPS surface and we see that R5L seems to have the ability to penetrate and rupture both lipids, but has the ability to do so to a greater extent in the more fluid DPPE:DOPS covered surface..... 36

**Figure 18:** AFM images of (a) a surface with just DPPE:DOPS, (b) Htau40WT on a surface covered in DPPE:DOPS, (c) R5L on a surface covered in DPPE:DOPS, and (d) a zoomed in image of the red box on (c). We can see from (a) that the lipid forms a uniform layer on the surface. From (b) and (c) we can see that both proteins have the ability to form oligomers, and even more importantly, on both, although to a greater extent in the presence of R5L, there is the formation of what could be pores in the lipid surface. .... 38

## LIST OF TABLES

<b>Table 1:</b> Kinetic parameters for protein adsorption to different surfaces .....	24
---	----



## ABSTRACT

The adsorption and aggregation of an intrinsically disordered soluble protein, tau, into insoluble filaments is a defining hallmark of many neurodegenerative diseases, commonly referred to as tauopathies. In its native state, the protein tau's function is to promote the assembly, and aid in the stabilization of microtubules. The microtubules allow for material transport through the axon, to and from the neuron. While the presence of aggregated tau protein fibrils are hypothesized to accelerate neuronal degradation, possibly by destabilizing microtubules, or disrupting cell membranes, more recent research has established the presence of soluble oligomeric species as being cytotoxic. These results necessitate a complete fundamental understanding of the governing principles that modulate the initial steps in the mechanisms of tau protein aggregation. The macromolecular environment, including the presence of surfaces such as the cell membrane, and the presence of macromolecules in a crowded environment, has been implicated in the aggregation of tau protein. However, the exact role of surfaces in modulating Tau protein aggregation has not been explored in detail. We hypothesize that Tau protein aggregation at model surfaces is modulated by two factors, the physicochemical properties of the surfaces, as well as the biochemistry of the protein molecules.

The work presented in this thesis project employs a combination of biophysical techniques to study the adsorption and aggregation of a wild type and several mutations of tau protein at model surfaces. A Quartz Crystal Microbalance with Dissipation (QCM-D) was used to monitor the adsorption of different tau species at nanomolar concentrations, mimicking the *in vivo* situation, to surfaces with different surface charge, wettability and softness, while Atomic Force Microscopy (AFM) was utilized to obtain direct visualization of the proteins at these different surfaces. Our results indicate that the hydrophobic amino acid sequence in the microtubule binding region was the leading force driving the adsorption of tau proteins to different surfaces. Further, AFM images provided direct evidence of the presence of

oligomeric tau species at the interfaces, establishing that the solid surface did in fact provide a template for the tau protein to form aggregates. Adsorption of different tau protein mutants to phospholipid covered surfaces of different fluidity indicated that tau protein oligomers can also cause destabilization or disintegration of lipid bilayers. Such disintegration may well be the cause of observed cell death in several tauopathies.

In summary, this thesis establishes that both protein biochemistry and the physicochemical properties of the surface modulate surface mediated aggregation. The work described in this thesis also provides a foundation for further research focused on the role of surfaces as templates that mediate tau aggregation pathway in vivo. A complete understanding of the mechanisms of tau aggregation will ultimately lead to strategies for therapeutic solutions for neurodegenerative diseases.

# CHAPTER 1

## INTRODUCTION

*Alzheimer's Disease:* Aggregation of soluble proteins into highly organized, insoluble, fibrillar structures both inside and outside the cell form a common pathology of many diseases (e.g., Alzheimer's, Parkinson's, and Huntington's disease, type II diabetes, liver cirrhosis and degenerative eye diseases)<sup>1</sup>.

Figure 1<sup>2</sup> shows examples of the tissue from different neurodegenerative diseases, sharing a commonality: aggregated protein structures that form the hallmark of these diseases.

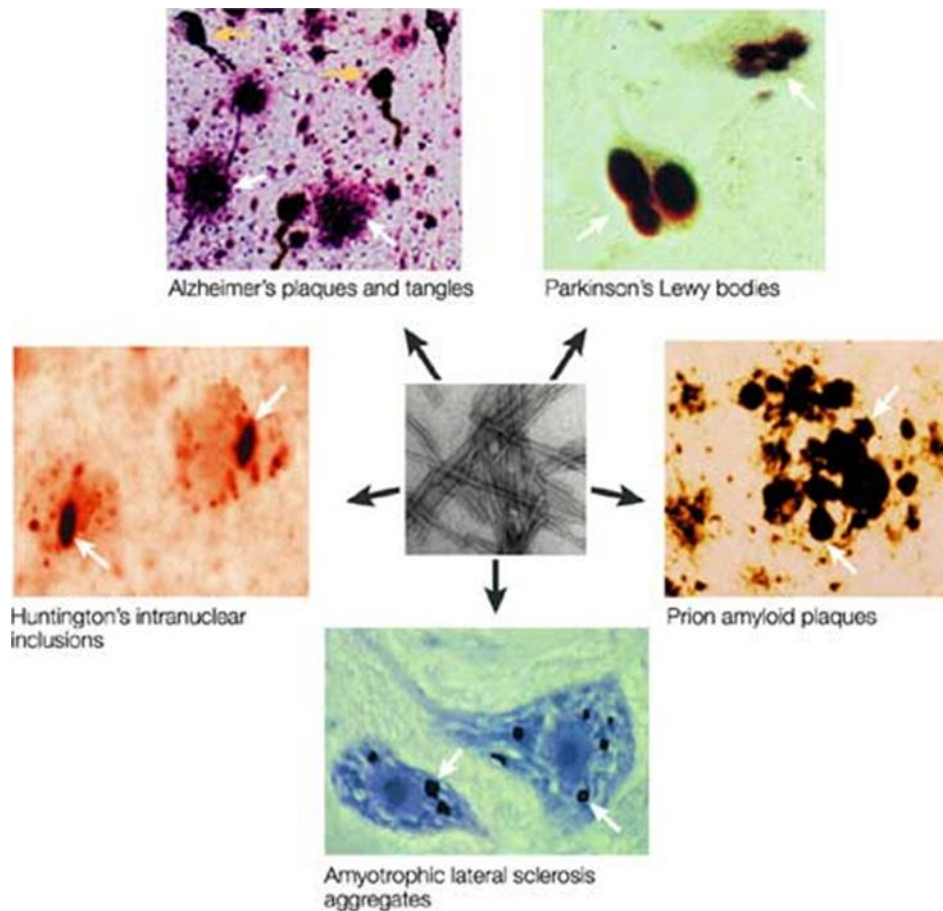


Figure 1: Hallmarks of Various Neurodegenerative Diseases<sup>2</sup>(with Permission from Nature Reviews Neuroscience)

For instance, Alzheimer's disease (AD) is a progressive neurodegenerative disease of the human brain, characterized by the accumulation of extracellular amyloid plaques and intracellular neurofibrillary tangles (NFTs). AD is the leading cause of all dementias, accounting for 60-80 percent of all cases,

typically affecting those 65 years of age and older<sup>3</sup>. In the earliest stages of AD, the part of the brain responsible for memory and learning is affected, and the disease then progresses from there to affect a much larger volume of the brain. By the time the disease has run its course, the brain volume, as seen in Figure 2<sup>3</sup>, has been decreased significantly due to the immense amount of cell death.

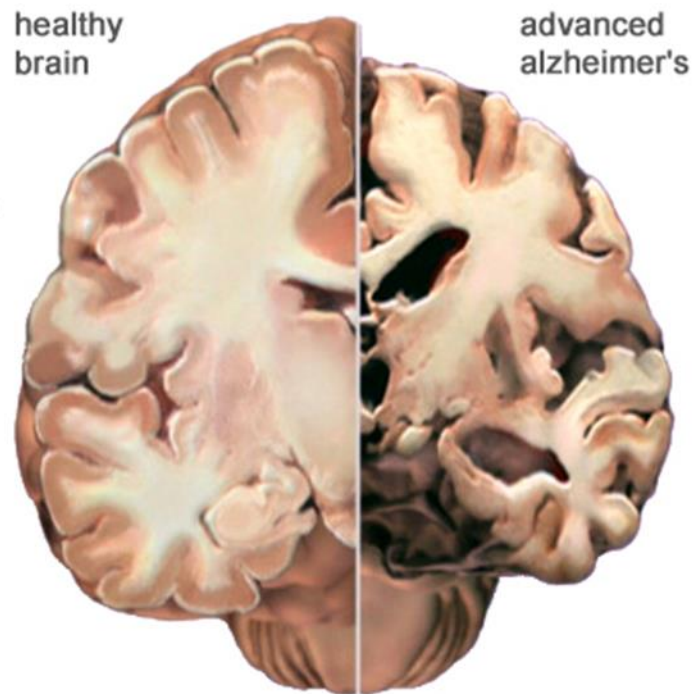


Figure 2: Brain Volume Comparison Between Healthy and Alzheimer's Brain<sup>3</sup>(©2015 Alzheimer's Association. [www.alz.org](http://www.alz.org). All rights reserved. Illustrations by Stacy Jannis)

*A $\beta$  and its role in AD:* It is now well established that the extracellular plaques, mentioned above, are a result of aggregation and accumulation of amyloid beta (A $\beta$ ) peptides<sup>4</sup>, which are a result of abnormal cleavage of the amyloid precursor protein (APP). APP is a transmembrane protein that is cleaved by two of three proteases:  $\gamma$ -secretase and either  $\beta$ -secretase or  $\alpha$ -secretase.  $\alpha$ -secretase cleaves the protein to form a relatively harmless peptide, while  $\beta$ -secretase cleaves the protein to form a longer peptide that is responsible for forming  $\beta$ -amyloid. These  $\beta$ -amyloid fragments aggregate together to eventually form the senile plaques found in the Alzheimer's Diseased brain<sup>3, 5</sup>. Figure 3 provides a visual for the mechanism leading to the amyloid plaques<sup>6</sup>.

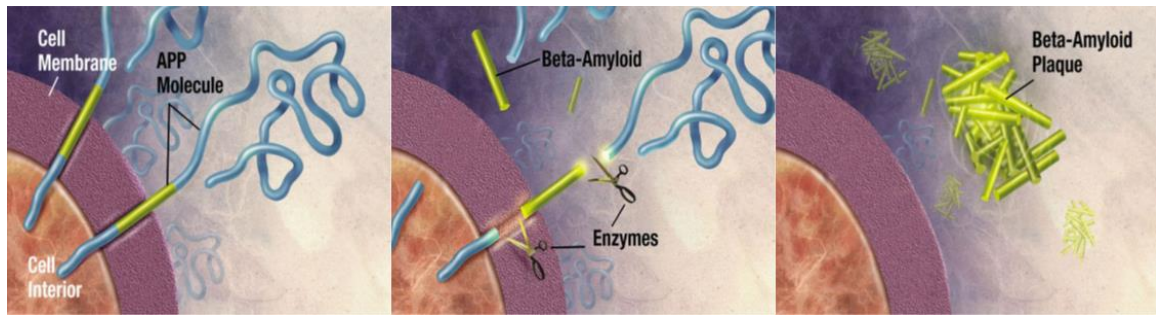
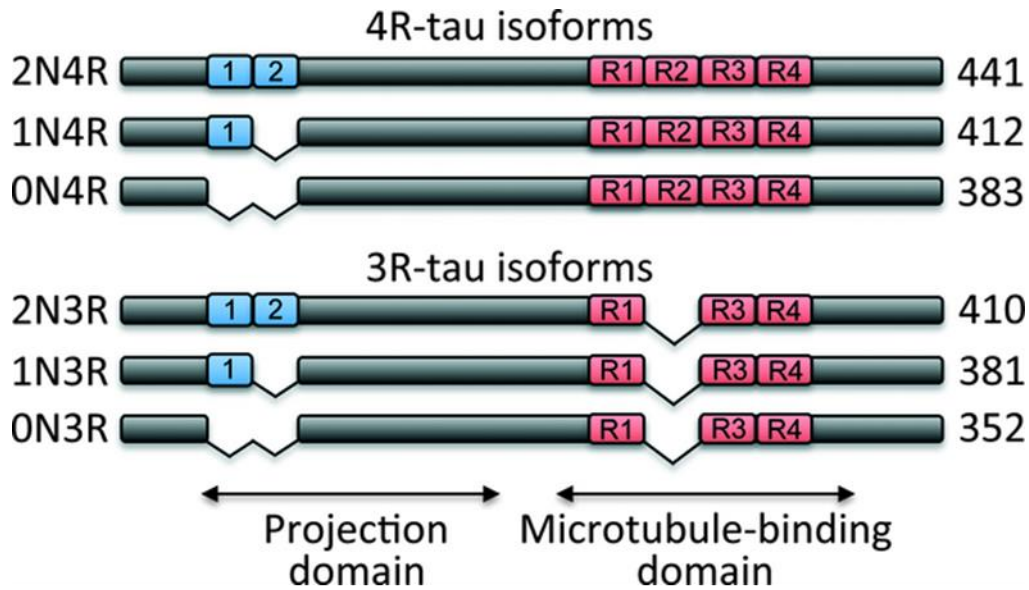


Figure 3: Mechanism of Amyloid Beta Formation<sup>6</sup>

*Tau protein and its potential role in AD:* The NFTs on the other hand are a result of aggregation of hyper-phosphorylated microtubule associated proteins called tau<sup>7</sup>. The tau protein in its native state promotes the assembly and aids in the stability of microtubules in human neuronal cells<sup>8</sup>. There are 6 isoforms of the tau protein, depending on how the mRNA is spliced, the longest form (2 N-terminus domains, 4 repeat domains; 441 amino acids) of which has the highest binding affinity for microtubules, and when found at an increased level can be a cause of neurodegeneration<sup>9</sup>. Figure 4 shows these 6 isoforms<sup>10</sup> along with the amino acid sequence, as well as the “paperclip” structure that the tau protein is hypothesized to take, along with its hypothesized mechanism for aggregation<sup>11</sup>.



1 maepraqefev medhagtygl gdrkdaggyt mhqdaqegtd aglkesplqt ptedgseepg  
 61 setsdakstp taedvtapl degapgkqaa aaphteipeg ttaeeagigd tpsledeaag  
 121 hvtqarmvsk skdgtgsddk kaggadgkik iatprgaapp gqkqanatr ipaktppapk  
 181 tppssgeppk sgdrsgyssp gspgtogrs rtpslptppt repkvavvr tppkspssak  
 241 srlatavpvm pdlknvski gstenlkhq gggkqvaiink kldlsnvask cgskdnikhv  
 301 pgggsvaivy kpvdlskvts kcgslgnihh kpgggqavek sekldfkdrv qskigsldni  
 361 thvpgggknk iethklfre nakaktdhga eivykspvvs gdtsprrhln vsstgsidmv  
 421 dspqlatlad evsaslakqg

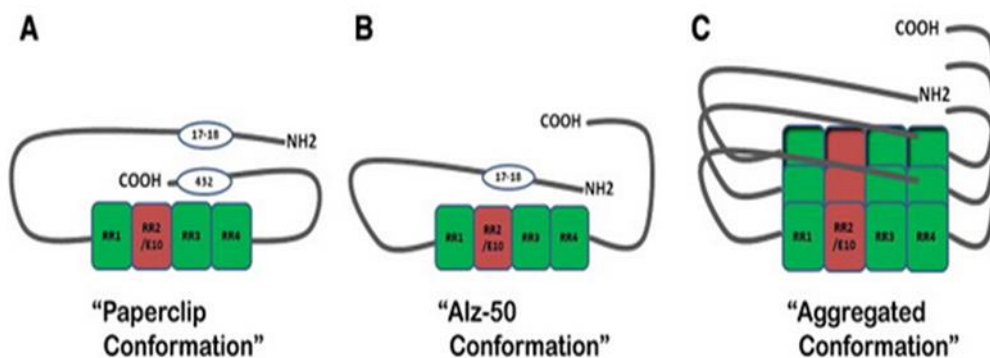


Figure 4: Tau Isoforms<sup>10</sup>, amino acid sequence, and Possible "Paper clip" Conformation and Hypothesized Aggregated Structure<sup>11</sup> (with permission from Journal of Neurochemistry, and Pharmacology and Therapeutics)

When tau proteins release from the microtubules, which is hypothesized to be due to the protein somehow becoming hyper-phosphorylated which weakens its binding ability<sup>12</sup>, the unbound proteins are then capable of forming the filamentous inclusions that are the hallmark of diseased Alzheimer's brain.

*Mechanisms of Protein Aggregation:* A multitude of experimental studies focused on fibrillization of different soluble proteins, including A $\beta$  and Tau, into insoluble protein aggregates lead to the following question: *in vivo*, what factors direct the self-assembly of these soluble proteins into insoluble aggregates, even at nanomolar concentrations, that are several orders of magnitude below the solubility limit of these proteins *in vitro*? One of the most prevalent explanations is the possible role of macromolecular crowding effects in the cellular environment that may enable directed self-assembly of these proteins by altering the local concentration. The cellular environment is also particularly rich in surfaces, including cell membranes and other macromolecules like glycans and proteins that provide large surface areas. Such local increases in the surface area provided by surfaces, reduce a three dimensional bulk space to a two-dimensional search and has also been hypothesized to enable protein aggregation. Indeed, cell membranes have been shown to assist in fibril formation in several different soluble proteins at nanomolar concentration relevant to the *in vivo* situation including A $\beta$  proteins,  $\alpha$ -synuclein, and huntingtin<sup>13, 14, 15</sup>. Therefore, the role of both hard and soft (lipid bilayer covered) surfaces have been the focus of this thesis.

*Rationale behind studying the aggregation of Tau:* A wide body of early research considered the amyloid plaques to be the primary cause of cell death<sup>16</sup>. For example, the introduction of amyloid beta has been shown to cause neuronal loss in several animal model studies<sup>17, 18, 19</sup>. As a result, most therapeutic approaches initially focused on A $\beta$  related pathology, causing tau-based therapies to lag behind<sup>20</sup>. However, failure of A $\beta$  pathology based treatments has now led to the realization that focusing on tau-related pathology is also critically important to advance treatments in AD and other neurodegenerative diseases<sup>20, 21</sup>. As a result, the structure of the final aggregated state of tau protein fibrils has been studied extensively. However, neuropathological analysis of the brains of patients with AD showed no direct correlation between the presence of amyloid plaques or NFTs and cognitive severity<sup>22</sup>. Such observations,

coupled with observations that purified oligomeric species and protofibrils exhibit greater cytotoxicity than mature fibrils have led to a shift in focus, emphasizing the possible role of soluble protein oligomers in causing neuronal injury and synaptic dysfunction. While more recent studies have focused on the formation of protein oligomers, and their potential toxic effects, and the role of inducer molecules in tau protein aggregation is recognized, most current research focused on tau protein aggregation does not focus on understanding surface induced mechanisms of protein oligomer formation. The work described in this thesis is motivated by the hypothesis that understanding the role of soft and hard surfaces as templates for aggregation is critical to understanding and potentially preventing protein aggregation.

*Role of Surfaces in Protein Aggregation:* Several *in vitro* studies have provided evidence of surface induced aggregation of amyloid proteins, particularly for A $\beta$ <sup>23, 24, 25</sup>. Using several different surfaces with varying hydrophobicity and hydrophilicity, and A $\beta$  as their model protein, Shen et al recently showed that surface enabled diffusivity of the protein oligomers are essential for fibril formation<sup>26</sup>. Giacomelli and Norde have shown that in addition to the hydrophobicity/hydrophilicity, electrostatic interactions with surfaces (silica surface with a net negative surface charge) can help control the structure of A $\beta$  proteins<sup>27</sup>. Saraiva et al. compared surface induced aggregation of A $\beta$ 40/42 and showed that A $\beta$ 42, but not A $\beta$ 40, formed viscoelastic protein oligomers at polystyrene and silica surfaces<sup>28</sup>. Therefore, based on the current literature, it is expected that both the nature of the protein as well as the nature of the surfaces contributes to surface mediated aggregation.

*Role of Lipids in Protein Aggregation:* As mentioned earlier, several recent studies have looked further into how protein aggregation is affected by the presence of lipids due to their abundance in the cellular environment. A recent study by Kunze et al. concluded that tau protein acts similarly to amyloidogenic peptides, which upon interaction with the membrane, adopt a more well-ordered structure, proposing a common mode by which these aggregates execute their toxic potential<sup>29</sup>. However, as with most of the current research in this area<sup>30, 31</sup>, only a fragment of the full length tau protein was used. To the best of our knowledge, we are aware of only one published study<sup>32</sup>, that used the full length, 441 amino acid, human



tau protein, to study its interactions with a model single component phospholipid monolayer. Moreover, we are not aware of any studies that focus on the interactions of different full length tau mutants with phospholipids. Therefore, we chose to use a full length tau protein along with two with mutants in either the binding domains or the N-terminus as our model proteins of interest. Further, some of these studies using lipids that have been reported, have shown that tau has some ability to adsorb and aggregate to zwitterionic lipids, but when the concentration of anionic lipids is introduced and increased, the tau proteins are much more likely to interact with the membrane and aggregate<sup>30,32</sup>. This is interesting since it has been seen that in Alzheimer's diseased brain, the amount of phosphatidylserine (PS), an anionic lipid, is found at an increased level<sup>33</sup>. Because of this fact, along with the fact that phosphatidylethanolamine (PE) is one of the most common lipids found in the cell membranes of neurons, the cells affected by AD, the lipid mixtures used in this work contained both of these. Further investigation into the characteristics of the membrane that might influence the tau's ability to aggregate could help us better understand the mechanism by which this toxic phenomenon occurs.

*Role of Surfaces in Protein Aggregation:* Several *in vitro* studies have provided evidence of surface induced aggregation of amyloid proteins, particularly for A $\beta$ <sup>23, 24, 25</sup>. Using several different surfaces with varying hydrophobicity and hydrophilicity, and A $\beta$  as their model protein, Shen et al recently showed that surface enabled diffusivity of the protein oligomers are essential for fibril formation<sup>26</sup>. Giacomelli and Norde have shown that in addition to the hydrophobicity/hydrophilicity, electrostatic interactions with surfaces (silica surface with a net negative surface charge) can help control the structure of A $\beta$  proteins<sup>27</sup>. Saraiva et al. compared surface induced aggregation of A $\beta$ 40/42 and showed that A $\beta$ 42, but not A $\beta$ 40, formed viscoelastic protein oligomers at polystyrene and silica surfaces<sup>28</sup>. Therefore, based on the current literature, it is expected that both the nature of the protein as well as the nature of the surfaces contributes to surface mediated aggregation.

*Project Focus:* Since the biochemical properties of the two AD-related proteins are significantly different, focusing on tau-related pathology of AD necessitates further understanding of the mechanisms of

aggregation of this protein. The research presented here is motivated by this need to study the mechanisms of AD-related tau proteins using hydrophobic and hydrophilic solid surfaces, along with simulated lipid membranes, as models of the crowded cellular environment. Because of the prevalence of the protein-lipid interaction, not only because of the cell membranes of neurons, but also because of the abundance of lipid layers due to macromolecular crowding within the cell, it was important to try to understand the mechanism behind the adsorption and aggregation of the tau protein at this surface. Microtubule associated protein, tau, in its normal soluble form predominantly binds to microtubules in axons and controls their assembly dynamics<sup>34, 35, 36, 37</sup>. In several neurodegenerative diseases including Alzheimer's disease, and tauopathies such as FTDP-17, the tau protein is modified, resulting in a reduced affinity for microtubule binding; instead the soluble tau protein monomers form soluble oligomers, insoluble filamentous structures, twisted paired helical filaments (PHFs) and non-twisted straight filaments (SFs)<sup>38, 39, 40</sup>. Human tau protein has six isoforms, that are differentiated by the presence of three or four repeat domains associated with binding to microtubules, as well as the presence and absence of one or two amino terminal inserts. Moreover, unlike the hydrophobic C-terminus of the short A $\beta$  proteins (40/42 amino acids), tau proteins do not have any *a priori* amyloidogenic sequences. Yet, *in vitro*, anionic inducer molecules including polyelectrolytes such as heparin, fatty acids such as arachidonic acid (ARA), anionic surfactants and carboxylate modified polystyrene beads have shown to induce aggregation of tau proteins<sup>41</sup>. Short patches at the beginning of the second (<sup>275</sup>VQIINK<sup>280</sup>) and third (<sup>306</sup>VQIVYK<sup>311</sup>) repeat units have been found to form the core of these aggregated structures, implicating the binding units in tau aggregation<sup>42, 43</sup>. However, the mechanisms of surface mediated aggregation of tau proteins, particularly the role of different surfaces, currently remains unexplored and forms the main motivation of this study.

In this thesis project, using Quartz Crystal Microbalance with Dissipation (QCM-D), we monitored the adsorption and binding of wild type full length human tau protein (WT Htau40) and an assembly incompetent protein (AIP) at three model solid surfaces, and the wild-type along with an N-terminus mutation (R5L) at two different model lipid membrane surfaces. We chose the wild-type protein so we could try to accurately identify characteristics of adsorption and aggregation that would be relevant in the

human neurons; we chose to use AIP to determine if the characteristics of the microtubule binding region was a main contributor to the protein's self-adsorption and aggregation; and finally, because the N-terminus is believed to be the section of the protein responsible for interacting with lipid membranes as well as play a role in the protein aggregation, we used R5L, which has been shown to increase the protein's nucleation rate<sup>44</sup>, for our lipid studies. Fig. 5 is a Kyte & Doolittle Plot<sup>45</sup>, which shows the hydrophobicity of every part of the protein sequence.

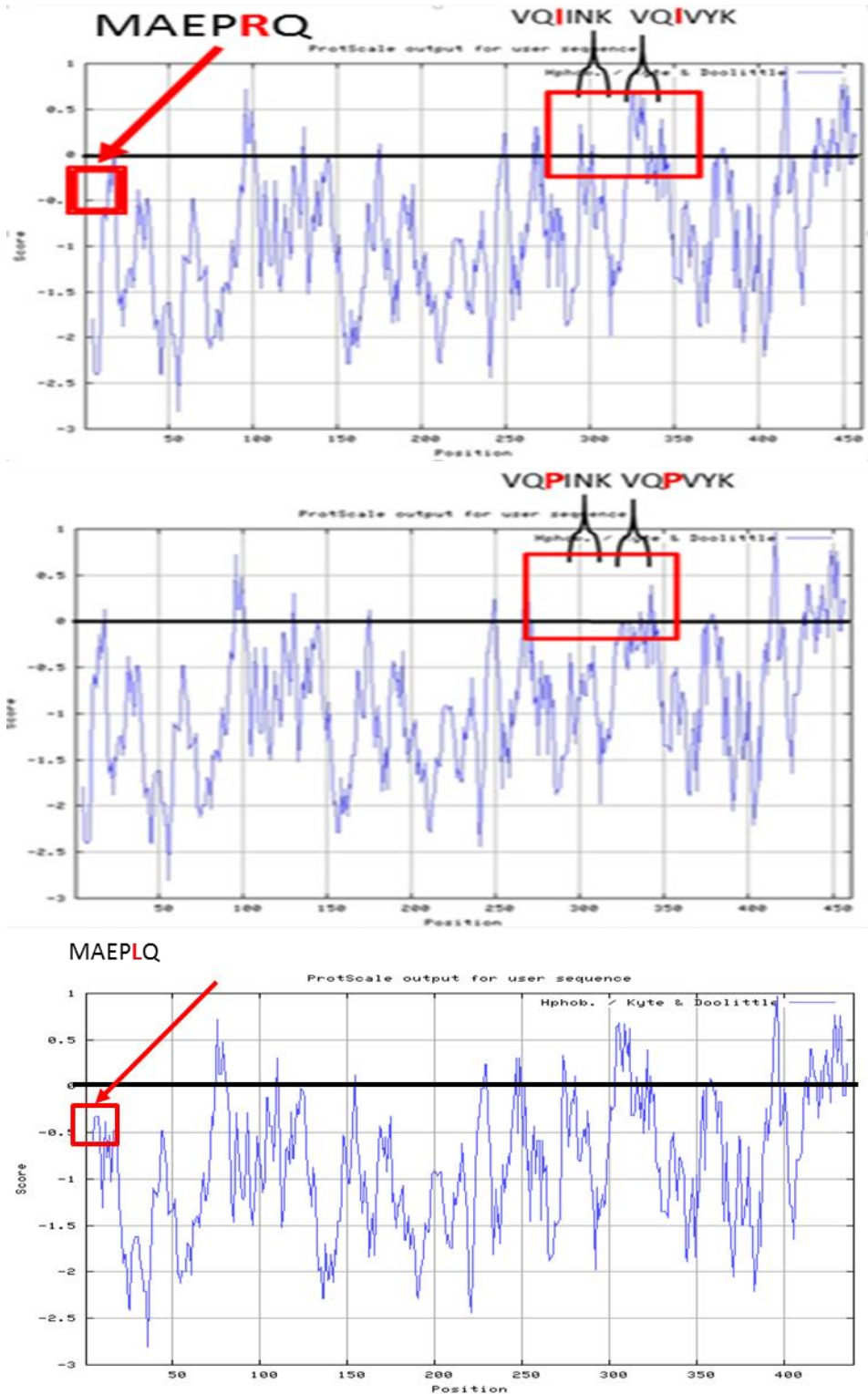


Figure 5: Kyte & Doolittle plots for (a) the wild-type protein, (b) AIP, and (c) R5L. Values close to 1 mean that a region is more hydrophobic. As can be seen in the figures, the location where the mutation in the binding region occurs is one of the most hydrophobic regions in the wild-type protein. This same region in the AIP is much less hydrophobic than the wild-type. For R5L, the mutation increases the hydrophobicity of the N-terminus.

In this plot, a value of 1 would be considered a hydrophobic region. Figure 5a shows that while the full length WT tau protein is primarily hydrophilic, the microtubule binding repeat (MTBR) region shows a slight hydrophobicity, because of the two hydrophobic sequences <sup>275</sup>VQIINK<sup>280</sup> and <sup>306</sup>VQIVYK<sup>311</sup> discussed before<sup>42, 43</sup>. By performing point mutations in this MTBR region, the hydrophobicity of the MTBR in the AIP was reduced as shown in Figure 5b. This mutation has been shown to prevent fibril formation in several previous studies. Further, Figure 5c shows that the point mutation in the 5<sup>th</sup> position of R5L has increased the hydrophobicity of the N-terminus slightly. This mutation, as stated previously, allows the R5L to nucleate at a higher rate than the wild-type protein.

*Choice of templates that serve as “inducers” of protein aggregation:* Motivated by studies using hydrophobic surfaces including polystyrene beads<sup>46</sup> as templates for aggregation, we used polystyrene as a model hydrophobic surface with no electrostatic charges<sup>47</sup>. Silicon dioxide was used as a model hydrophilic surface with negative surface charges, while gold sensors were used as a control electrostatically neutral system with moderate hydrophobicity. The two lipid membranes that were used were a 4:1 ratio of 1,2-dipalmitoyl-*sn*-glycero-3-phosphoethanolamine(DPPE):1,2-dipalmitoyl-*sn*-glycero-3-phospho-L-serine(DPPS) and a 4:1 ratio of DPPE:1,2-dioleoyl-*sn*-glycero-3-phospho-L-serine(DOPS). As mentioned previously the phosphatidylethanolamine (PE) and phosphatidylserine (PS) were chosen because they are common in the part of the brain affected by Alzheimer’s Disease and the DOPS was interchanged with the DPPS to determine the affect of adding an unsaturation to the tail region of the lipid. The possible presence of oligomeric species was further monitored, on the bare surface experiments, by recording the binding of thioflavin to different protein covered surfaces. Finally these QCM-D studies were complemented with direct high resolution imaging of the proteins at the different surfaces using atomic force microscopy (AFM). Together, our results present a detailed understanding of the mechanisms of Tau protein adsorption and binding to solid surfaces as well as the mechanisms of surface mediated aggregation of an intrinsically disordered protein.

## CHAPTER 2

### MATERIALS AND METHODS

**Chemicals:** Ethylenediaminetetraacetic acid (EDTA), 4-(2-hydroxyethyl)-1-piperazineethanesulfonic acid (HEPES), and Sodium chloride (NaCl) used for the preparation of buffer were purchased from Fisher Scientific, while the Dithiothreitol (DTT) and Thioflavin (ThT) were purchased from Sigma-Aldrich. All water (resistivity 18.2 M $\Omega$ /cm) used for these experiments was obtained using a Millipore Gradient water purification system (Billerica, MA). Hellmanex III solution, used for cleaning the QCM-D sensors, was purchased from Hellma, while all organics used for cleaning the sensor surfaces were purchased from Fisher Scientific. Polystyrene used for creating hydrophobic surfaces was purchased from Sigma-Aldrich.

**Surfaces:** The sensors used for QCM-D experiments of protein and lipid adsorption to different surfaces include gold, polystyrene and silicon dioxide surfaces, purchased from Biolin Scientific. The QCM-D sensors consist of a piezoelectric, AT-cut quartz crystal with a fundamental frequency of 5 MHz, sandwiched between two gold electrodes with or without surface modifications (polystyrene and silicon dioxide). Since the QCM-D sensors were too rough for AFM imaging, smooth Silicon dioxide wafers (University Wafer) were used for the AFM studies described here. The silicon dioxide wafers were cut with a diamond cutter to provide roughly 1cm by 1cm pieces and used without further modifications for imaging the proteins on silicon dioxide surfaces. A hydrophobic polystyrene surface was created in-house by completing the following protocol. A 10 wt % solution of polystyrene in toluene was spun onto the previously cut silicon dioxide wafers at a rate of 2500 rpm for 30 seconds<sup>48</sup>, and then baked for 20 minutes at 50°C to obtain a uniformly coated polystyrene surface. The uniform coating of polystyrene was verified by AFM imaging.

**Proteins:** Wild type, R5L and I277, 308P (Assembly incompetent) tau in 2N4R tau protein (441 amino acids) were cloned into a PT7c vectors with an N-terminal polyhistidine tag as previously described<sup>49, 50</sup>. The proteins were isolated by affinity chromatography through an Ni NTA Agarose (Qiagen, Valencia, CA) column followed by gel filtration through a Superdex 200 column on AKTA fast protein liquid

chromatography (FPLC) (Amersham Biosciences, Piscataway, NJ) as described previously<sup>51</sup>. These proteins were prepared by Smita Paranjape from the Department of Molecular Biosciences at KU.

*Lipids:* Lipids DPPE, DPPS, and DOPS (Structures shown in Figure 6), in chloroform were purchased from Avanti Polar Lipids. The Texas Red dye was purchased from Invitrogen. The lipid solutions were prepared by combining DPPE:DOPS in a 4:1 ratio as well as combining DPPE:DPPS in a 4:1 ratio.

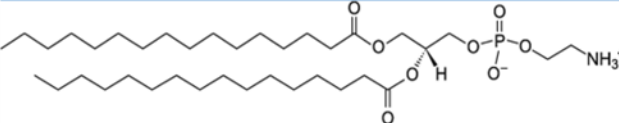
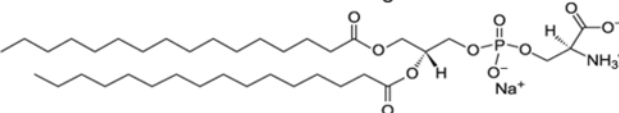
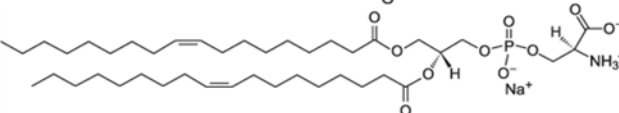
Lipid Name	Lipid Structure
<b>1,2-dipalmitoyl-<i>sn</i>-glycero-3-phosphoethanolamine (DPPE)</b>	
<b>1,2-dipalmitoyl-<i>sn</i>-glycero-3-phospho-L-serine (DPPS)</b>	
<b>1,2-dioleoyl-<i>sn</i>-glycero-3-phospho-L-serine (DOPS)</b>	

Figure 6: Lipid structure of DPPE, DPPS, and DOPS

Texas Red was then added as one percent of the combined weight of the lipid mixture. The lipids were then dried using nitrogen gas to evaporate the chloroform, and stored under vacuum overnight to remove any residual organic solvents. Polymerization buffer (for QCM-D experiments) or MilliQ water (for AFM experiments) was used to hydrate the lipids to a final concentration of 5 mg/ml solution of the lipids by incubating the lipids in the buffer or water solutions overnight in a water bath held at 65° Celsius. This high temperature was maintained to ensure that temperature higher than the melting temperature of the lipids was always maintained. . To ensure that the lipid solution was uniformly hydrated, the solution was subjected to intermittent shaking every 30 minutes for the first 3 hours, using a vortex. Following hydration, the lipids were diluted to 1 mg/ml. At this point, the lipids exist as multi lamellar vesicles (MUVs). In order to obtain unilamellar vesicles, the lipid solution was subjected to pulse sonication using a point sonicator from Fisher Scientific, for 10 minutes at 40% amplitude with a second long pulse every

other second. The solution was then centrifuged for 30 minutes to remove any titanium particles from the tip sonicator, and finally diluted to a concentration of 0.1 mg/ml.

*QCM-D*: A Q-Sense E4 QCM-D was used for all mass adsorption data presented here. The E4 model consists of four modules, allowing simultaneous recording of four different measurements. Before beginning recording the adsorption of the lipid or the protein Tau onto the different surfaces of interest, the QCM-D sensors were thoroughly cleaned to remove any organic impurities and ensure maximum adsorption of the lipids or proteins to a clean surface, by following the protocol described below. UV/Ozone ProCleaner from Bioforce Nanosciences was first used to remove any organic impurities from the gold and silicon dioxide sensor, by leaving them in the chamber and exposing them to UV light for ten minutes. This treatment with UV/Ozone was not used on the polystyrene sensors, because the ozone treatment can potentially reorganize the polystyrene substrate and alter its hydrophobicity<sup>52</sup>. The sensors were then placed in a sample holder, immersed in an ethanol bath, sonicated for ten minutes, washed several times in MilliQ water, and dried under a nitrogen stream. The gold and silicon dioxide sensors were then placed back in the UV/Ozone chamber for another ten minutes, before they could be taken out for use. All cleaned sensors were placed in the QCM-D module and mounted onto the QCM-D chamber for further cleaning and analysis. Initially, 100 mL of a 2% by volume Hellmanex solution was pumped at 0.50 ml/min through the modules kept in a chamber maintained at 30 °C, to enable further cleaning of the sensors and the sample chambers. After ensuring that the flow of the solution had completely filled the modules, the oscillations of the system were calibrated to within 20% of the given dissipation values to ensure there were no air bubbles and the instrument was set to record changes in the frequency and dissipation. A saturation in the frequency and dissipation values suggested no further addition or removal of surfactant. At this point, the sample chambers, sensors, and tubing were washed thoroughly by pumping MilliQ water through the instrument for one hour or more until there was no further change in the frequency and dissipation. Next, the sensors were equilibrated with a polymerization buffer (100 mM NaCl, 10 mM HEPES, 0.1 mM EDTA and 5 mM DTT) at a flow rate of 0.10 ml/min for around 15 minutes at a temperature of 25 °C for the experiments of protein adsorption on bare surfaces and 37°C for



the experiments of protein adsorption to lipid saturated surfaces. For the protein adsorption to bare surfaces, calculated concentrations of the protein solutions in the polymerization buffer were next pumped through the sensors for ten minutes, to ensure that the protein solution filled the modules as well as the piping system, and then the pumping stopped. For the experiments involving the lipid solutions, the lipid solution was first pumped through following the polymerization buffer for 20 minutes, and the pump was then stopped for another 20 minutes. The proteins were then pumped through, following the same procedure mentioned above. The sensors were allowed to sit in this protein solution overnight (20 hours), and the changes in the frequency and dissipation recorded continuously during this time. Acetate buffer (at pH 7.4) was pumped through the sensor chambers to remove any unbound proteins while maintaining the pH of the environment. Finally, for the proteins on bare surfaces, 2 mg/ml of ThT in acetate buffer was pumped over the sensors for thirty minutes to record the possible formation of oligomeric species.

*AFM:* A Veeco diMultimode V microscope with a J-scanner (XY scan range of 125x125 microns) was used in tapping mode for all imaging experiments. Antimony doped Silicon probes (Bruker Scientific) with a resonant frequency around 371 kHz were used as tapping mode probes for these imaging studies. To ensure identical conditions in the two experiments, the same protein incubation protocol was followed for the silicon-dioxide and polystyrene coated wafers used for the AFM experiments and the QCM-D sensors used in the mass adsorption studies. The wafers were first cleaned following the protocol used to clean the QCM-D sensors, and then, for the samples not containing lipids, the wafers were allowed to sit in a 450 nM solution of proteins in the polymerization buffer for 20 hours at 25 °C. For the samples containing lipids, an additional step was added before the protein incubation. The wafers were heated on a hot plate above the melting temperature of the lipid mixtures, and then subsequently covered in the lipid solution. As the solution dried, the lipid vesicles opened up to form bilayers that settled onto the wafer surface. This surface was then imaged using a fluorescence microscope to confirm that a lipid layer had indeed deposited. These surfaces, now covered with a lipid bilayer, were then placed into the protein solution for 20 hours at 25°C. Next, the sensors were washed in acetate buffer to remove any deposited salts and unbound proteins, while also ensuring that the acidity of the protein's solvent environment did

not change. Such precaution is necessary, since a) an alteration of pH can alter the structure of the protein, b) presence of salt crystals can lead to erroneous images. The wafer pieces were dried under a gentle stream of nitrogen and imaged immediately. For the AFM imaging, a one micron by one micron area was used, and the scan speed was set at 1 micron per second, such that 512 pixels were recorded per line. Once an image was generated, it was saved and the probe was withdrawn from the surface and moved to a different section of the sample. At least three representative images were recorded for each protein solution and for each sensor. Additionally, polystyrene and silicon dioxide wafers incubated with the polymerization buffer for twenty hours, without proteins or lipids, cleaned with acetate buffer, and dried under nitrogen were used as control samples.

*Analysis of the QCM-D data:* QCM-D offers a technique sensitive enough to record the adsorption of even picograms of proteins in solution to surfaces with different surface modifications. QCM-D uses the oscillation of a piezoelectric quartz crystal to directly measure the frequency of oscillation and the dissipation of energy due to the physical properties of the adsorbed layer. The change in frequency measures how the oscillation rate changes as mass is adsorbed to, or removed from the surface. As mass is added, the crystal will become heavier, causing the oscillations to decrease. This frequency decrease allows for the detection of a mass increase. The QTools software, available with the instrument, allows one to relate the changes in frequency and dissipation to quantitative values of mass adsorbed with very high sensitivity. Briefly, for a rigid layer, Sauerbrey's equation gives a linear relationship between the changes in frequency and the total mass of molecules adsorbed onto a sensor surface. However, for many systems, like the proteins adsorbing in a fluid environment, the layer of protein at the surface showed a viscoelastic characteristic (non-zero values for dissipation change). In such situations, the Sauerbrey equation cannot be used. Instead, the QTools software was used to calculate the mass of protein adsorbed, by fitting the frequency and dissipation data to the Kelvin-Voigt model developed by Kasemo and coworkers and now available as a built-in model in QTools<sup>53, 54</sup>. The following equations are used in QTools to relate the change in frequency and dissipation to changes in the height and mass of the adsorbed layer.

$$\Delta f \approx -\frac{1}{2\pi\rho_0 h_0} \left\{ \frac{\eta_3}{\delta_3} + h_1 \rho_1 \omega - 2h_1 \left( \frac{\eta_3}{\delta_3} \right)^2 \frac{\eta_1 \omega^2}{\mu_1^2 + \omega^2 \eta_1^2} \right\} \quad (1)$$

$$\Delta D \approx \frac{1}{\pi f \rho_0 h_0} \left\{ \frac{\eta_3}{\delta_3} + 2h_1 \left( \frac{\eta_3}{\delta_3} \right)^2 \frac{\eta_1 \omega}{\mu_1^2 + \omega^2 \eta_1^2} \right\} \quad (2)$$

$\Delta f$  in equation 1 is the frequency change of the system,  $\Delta D$  in equation 2 is the dissipation change of the system,  $\rho_0$  and  $\rho_1$  are the densities and  $h_0$  and  $h_1$  are the heights of the crystal and the adsorbed layer respectively.  $\eta_1$  is the viscosity of the adsorbed layer, while  $\eta_3$  is the viscosity of the bulk fluid. Using estimated values of the density and viscosity of the bulk fluid solution as user inputs, the height and density of the protein layer was obtained as fitting parameters. Equation 3 was then used to calculate the mass per area adsorbed.

$$\Delta m = h_1 \times \rho_1 \quad (3)$$

Additionally, the ability to record the different overtones allow further analysis of the viscoelastic data. Since the penetration depth of the acoustic waves with respect to different overtones are different, the higher overtones are representative of the processes closer to the surface of the sensor, while the lower overtones represent processes at the fluid/film interface. The analysis presented here used the fifth overtone for all calculations. Further, if the  $f$  and  $d$  values overlap for the different overtones, this indicates a homogenous coverage on the surface with similar properties.

## CHAPTER 3

### RESULTS AND DISCUSSION

The research presented here is focused on addressing the need to understand the role of surfaces, as well as the hydrophobicity of the protein in modulating the adsorption and aggregation of Tau, in order to better understand the aggregation of Tau proteins that forms a defining hallmark of several neurodegenerative diseases<sup>55</sup>. The rest of this chapter focuses on understanding the adsorption of different tau proteins on bare and lipid covered interfaces as models for hard and soft surfaces.

#### **3.1-Protein Adsorption to solid surfaces:**

In this part, we present the effect of both the differences in the surface properties as well as the protein biochemistry to better understand the interactions governing Tau protein adsorption and aggregation at different solid surfaces. Particularly, a polystyrene surface was used as a model hydrophobic surface, while silicon dioxide was used to represent a hydrophilic surface with a net negative charge. Further a gold surface was used as a neutral surface with an intermediate hydrophobicity. The hydrophobicity of the two proteins of interest, WT and AIP tau are shown by Kyte & Doolittle<sup>45</sup> plots in Fig. 5. A value of one in these plots is considered to be for hydrophobic amino acids, while a value of zero indicates primarily hydrophilic amino acids.

In order to determine the potential saturation concentration to be used for all studies, the adsorption of several different concentrations of WT tau below 1 mM to a hydrophobic polystyrene surface were monitored. Figure 7 shows the maximum change in frequency (Fig. 7a) as well as the mass adsorbed (Fig.7b) as a function of wild-type Tau protein concentration, when incubated with a hydrophobic polystyrene surface. Fig.7 (a-b) show that the maximum change in frequency and therefore the mass of protein adsorbed increased with increasing protein concentration, until a saturation value was reached for concentrations over 450nM. Therefore, this concentration was used to compare the differences in the adsorption of the WT and assembly incompetent proteins to the different surfaces. It is important to note

that this concentration is at least an order of magnitude below the concentrations typically used for *in-vitro* inducer molecule induced tau aggregation studies.

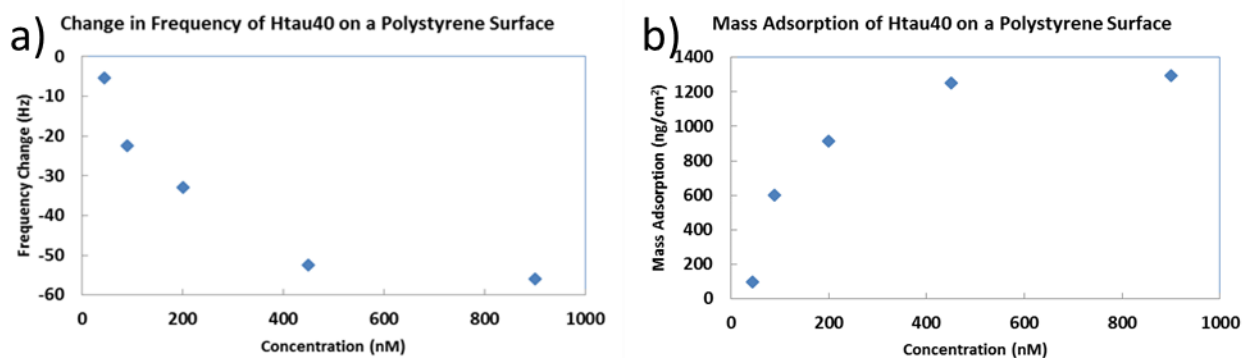


Figure 7: (a) Maximum change in Frequency and (b) maximum calculated adsorbed mass of Htau40WT on Polystyrene as a function of protein concentration, showing a saturation in protein adsorption beyond 450nM protein concentration

**Adsorption of WT Tau to hydrophobic vs. hydrophilic surfaces:** The QCM-D technique employed here allows sensitive *in situ* measurements of protein adsorption and binding to different surfaces. As noted above, QCM-D gold sensors coated with polystyrene and silicon dioxide served as hydrophobic and hydrophilic<sup>56</sup> surfaces, while the gold sensors were used as a control intermediate surface<sup>47</sup>. After thorough cleaning and exposure to water or air, the silicon oxide surface is saturated with silanol (Si-OH) groups that impart a negative surface charge with constant surface charge density in the pH range of 3-8<sup>28</sup>. Since the WT protein has a net positive charge at pH 7.4<sup>57</sup>, the silicon dioxide sensor can also be used to study the effect of electrostatic interactions on Tau protein adsorption and aggregation at surfaces. Fig. 8 shows the differences in the change in frequency (Fig. 8a) and change in mass (Fig. 8b) as a function of time when 450 nM WT Htau40 was allowed to incubate with polystyrene, gold, or silicon dioxide surfaces in the absence of any shear flow. The results presented in Fig. 8(a,b) indicate that for all the surfaces, the wild-type proteins adsorbed relatively quickly and reached a saturation value. The black line represents protein adsorption to a polystyrene surface, the red line represents protein adsorption to a silicon dioxide surface, and the blue line represents protein adsorption to a gold surface. For the wild-type, protein adsorption to the polystyrene surface reached a maximum frequency change of -52 Hz within one hundred minutes. In contrast, the lowest adsorption occurred on the silicon dioxide surface,

with a maximum value of frequency of -40 Hz. However, this maximum value was reached within only 3 minutes. For protein adsorbing to the gold surface, the change in frequency was the highest, and reached a maximum value of -60 Hz within 300 minutes. This suggests that the hydrophobic polystyrene and neutral gold surface reach saturation coverage much later than the hydrophilic and negatively charged silicon dioxide surface, even though the maximum adsorbed amounts are much lower on the silicon dioxide surface. Similarly, when comparing the hydrophobic polystyrene surface with the hydrophilic, but negatively charged silicon dioxide surface, the calculated mass adsorbed onto polystyrene was found to be higher than that adsorbed on silicon dioxide (1200 ng/cm<sup>2</sup> for polystyrene vs. 1000 ng/cm<sup>2</sup> on silicon dioxide surfaces). Interestingly, the mass of protein adsorbed onto gold was found to be almost twice as much (2000 ng/cm<sup>2</sup>) as that adsorbed to either of the modified surfaces.

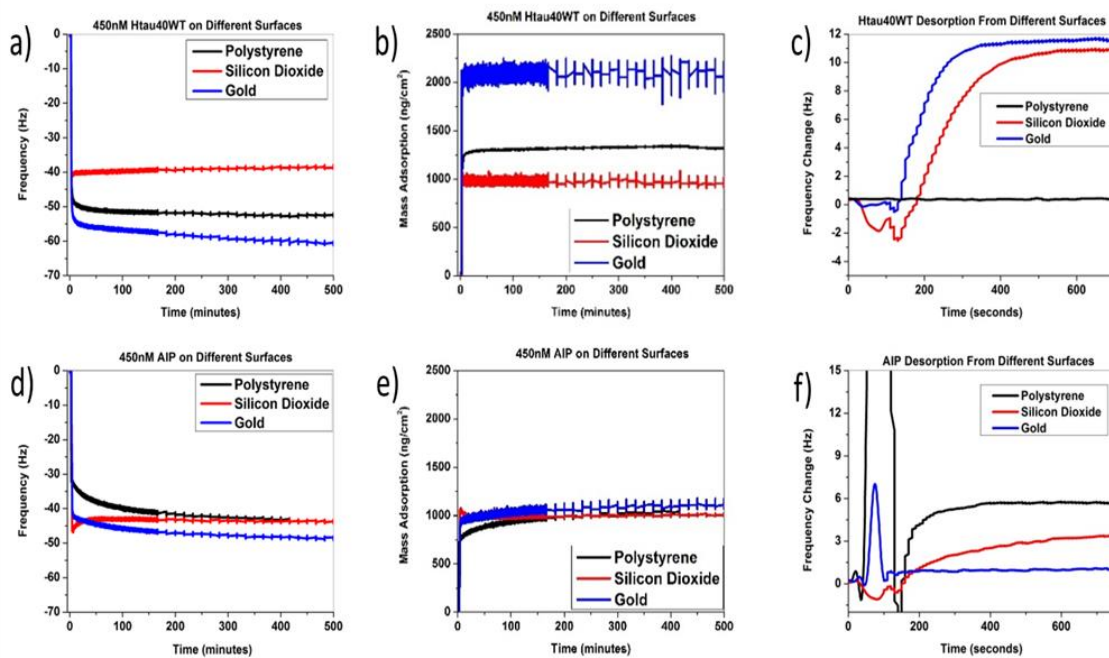


Figure 8: (a,d) Changes in frequency (Hz) and (b,e) changes in the calculated adsorbed mass (ng/cm<sup>2</sup>) of protein as a function of time during adsorption of 450nM Htau40WT (a,b) and AIP (d,e) on different surfaces (gold (blue), silicon dioxide (red), and polystyrene (black)). Figure 8 (c,f) represent changes in frequency due to protein desorption when buffer was run across surfaces saturated with Htau40WT (c) and AIP (f)

Washing the protein bound surfaces with buffer after the experiment provided further insight into binding affinity of tau to the respective surfaces. Fig. 8c shows the recorded changes in the frequency because of protein desorption, where an increase in the frequency implies desorption of material from the

surface. No loss of protein was noted in case of the polystyrene surface, and only a small loss of protein in case of the silicon dioxide and gold surfaces was noted, suggesting that while there was protein binding onto all surfaces, the proteins were bound more tightly to the hydrophobic surfaces. This increased binding to the hydrophobic surfaces may be understood by reviewing the hydrophobicity of the WT protein. As noted in the Kyte & Doolittle plots shown in Fig. 5 above, full length WT tau protein is primarily hydrophilic while, the microtubule binding repeat (MTBR) region shows a slight hydrophobicity. It is possible that this hydrophobicity of the MTBR caused more proteins to be attracted and bound to the hydrophobic polystyrene surface when compared with the hydrophilic silicon dioxide surface. However, when comparing the adsorption of Tau proteins to the intermediate control, the gold surface, we found that the amount of adsorbed protein was higher than both the hydrophobic and the hydrophilic surfaces. This suggests that the neutral and intermediate wettability of the Tau proteins induces maximum protein adsorption, even though the strength of the binding to the surface was found to be the maximum in case of the polystyrene surface. Similar behavior has been reported for amphiphilic A $\beta$  peptides adsorbing to surfaces with varying surface wettability<sup>26</sup>. A $\beta$  adsorption to highly hydrophilic surfaces did not form aggregated structures. At the same time highly hydrophobic surfaces were found to prevent fibril formation. Using single molecule tracking, Shen et al. concluded that the A $\beta$ 's ability to maintain sufficient translational mobility at a surface was critical to its forming aggregated fibrillar structures<sup>14</sup>. The ability to maintain sufficient translational mobility at the surface might also be the reason why Tau proteins show the maximum adsorbed mass onto the gold surface, by allowing migration of the proteins at the surface and therefore allowing more proteins to adsorb.

**Effect of protein biochemistry on protein adsorption to a bare surface:** To further test that the difference in htau40 WT adsorption to different surfaces was controlled by the hydrophobicity of the MTBR, an assembly incompetent protein (AIP) with no net hydrophobicity in the MTBR domain (Figure 5b) was also studied. Figure 8(d) is a plot of the frequency as a function of time for the adsorption of AIP to the three different surfaces, and Figure 8(e) is a plot of the calculated adsorbed mass as a function of

time for the same experiments. Similar to Fig. 8(a,b), in these plots the black line shows the adsorption of AIP to the polystyrene surface, the red line represents the adsorption to silicon dioxide, and the blue line represents the adsorption of AIP to the gold surface. AIP adsorbed to the polystyrene surface with a maximum change in frequency of -42 Hz within 200 minutes. AIP adsorption to the silicon dioxide surface was characterized by an initial peak in the change in frequency at -46 Hz within 4.5 minutes, followed by a slight decay to a saturation value at -43 Hz. AIP adsorbed to the gold surface with a maximum change of -48 Hz within 200 minutes. Therefore, comparing the change in frequency and mass of AIP adsorbing to the polystyrene, gold and silicon dioxide surfaces showed that unlike the case of the htau40 WT proteins, there was no significant difference when the AIP adsorbed to the different surfaces. Moreover, Fig 8(f) shows that when compared with the hydrophobic surface, AIP proteins desorb the most from the polystyrene surface, further alluding to the role of the hydrophobicity of the MTBR in modulating the strength of AIP binding.

Fig. 9(a-f) presents further comparison of the adsorption of WT Htau40 proteins and AIP to each of the surfaces: polystyrene, gold and silicon dioxide. Fig. 9(a, c, e) are plots of the change in frequency as a function of time due to protein adsorption, while Fig 9(b, d, f) are plots of the calculated adsorbed mass as a function of time. On these plots the black line represents the adsorption of the wild-type protein and the red line represents the adsorption of the AIP to each of the surfaces while the green line shows the kinetics of protein adsorption fitted using a double exponential decay. This direct comparison between the two proteins showed that for adsorption to both polystyrene and gold, the AIP had a decrease in the total adsorbed mass, when compared with the WT. However, for the hydrophilic silicon dioxide surface, no difference was noted between the adsorbed mass of WT or AIP.



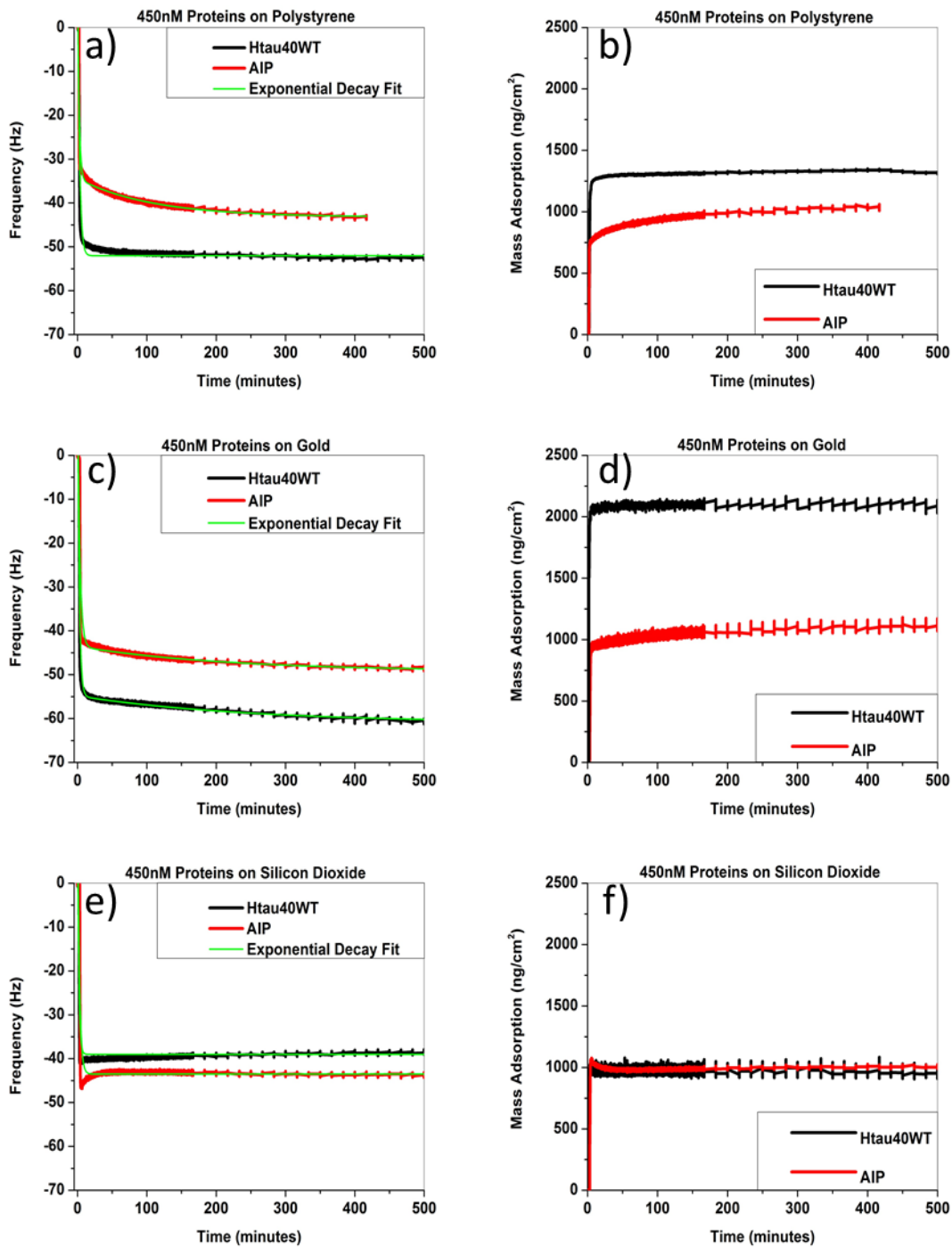


Figure 9: (a,c,e) change in frequency (Hz) as a function of time and (b,d,f) change in the calculated adsorbed mass (ng/cm<sup>2</sup>) as a function of time, during adsorption of 450nM Htau40WT (black) and AIP (red) proteins on polystyrene, gold, and silicon dioxide surfaces. The green curves show a fit to exponential decay curves, showing the kinetics of protein adsorption. The fitting parameters and goodness of fit are shown in Table 1.

Further, detailed results of the kinetic parameters obtained from fitting the change in frequency as a function of time are reported in Table 1. Analysis of these parameters shows that the kinetics of protein

adsorption depends on both the protein biochemistry, as well as the intrinsic properties of the surfaces. Adsorption of Tau proteins to a hydrophilic silicon dioxide surface can be described by a single exponential decay regardless of the protein biochemistry, even though the rate constant for adsorption is slightly higher for the WT htau40 proteins, when compared to the AIP. On the other hand, adsorption of proteins to the gold surface followed a two-step adsorption process regardless of the protein biochemistry. The single step for the adsorption suggests that the protein aggregation possibly occurs after the adsorption of the proteins has reached saturation, while the two step process suggests a possible rearrangement after initial adsorption. Further, for the hydrophobic polystyrene surface, WT proteins showed a one-step adsorption process, while the AIP showed a two-step adsorption.

**Table 1: Kinetic Parameters:  $\Delta F = A_1 e^{-k_1 t} + A_2 e^{-k_2 t} + \text{offset}$**

Experiment	A <sub>1</sub>	k <sub>1</sub>	A <sub>2</sub>	k <sub>2</sub>	offset	Goodness of Fit (R <sup>2</sup> )
<b>Wild-type on Polystyrene</b>	70.1041	0.3745			-52.0249	0.89
<b>Wild-type on Silicon Dioxide</b>	55.8537	0.5689			-39.0171	0.65
<b>Wild-type on Gold</b>	6.1670	0.0041	75.5163	0.4243	-60.9893	0.85
<b>AIP on Polystyrene</b>	8.7854	0.0093	47.1952	0.4593	-43.2090	0.94
<b>AIP on Silicon Dioxide</b>	63.2626	0.3776			-43.5179	0.80
<b>AIP on Gold</b>	60.4411	0.3134	5.6705	0.0047	-49.2004	0.91

*Table 1: Kinetic parameters for protein adsorption to different surfaces*

Interestingly, as shown in Fig. 10, we found that in case of both proteins, the ratio of  $\Delta D/\Delta f$  initially showed a linear increase, suggesting that the adsorbed proteins (and any protein oligomers forming at the surface) had a viscoelastic nature, irrespective of the nature of the protein. Moreover, the difference in the slope of the curves in case of a polystyrene surface (Fig. 10a) indicate that the more hydrophobic WT htau40 proteins form a softer layer than the AIP, possibly because AIP proteins do not form many oligomeric species. No differences in the slopes were recorded for the gold (Fig. 10b) and silicon dioxide (Fig. 10c) surfaces, indicating that the hydrophobic surface has a stronger influence on the viscoelastic properties of the proteins at the surfaces. This behavior is in contrast with amphiphilic A $\beta$  peptides. Previous studies by Saraiva et al. have reported that amphiphilic A $\beta$ 42 peptides adsorbing to polystyrene

and silicon dioxide surfaces were viscoelastic, but this soft behavior was not observed for the A $\beta$ 40 peptides (which are less hydrophobic)<sup>58</sup>.

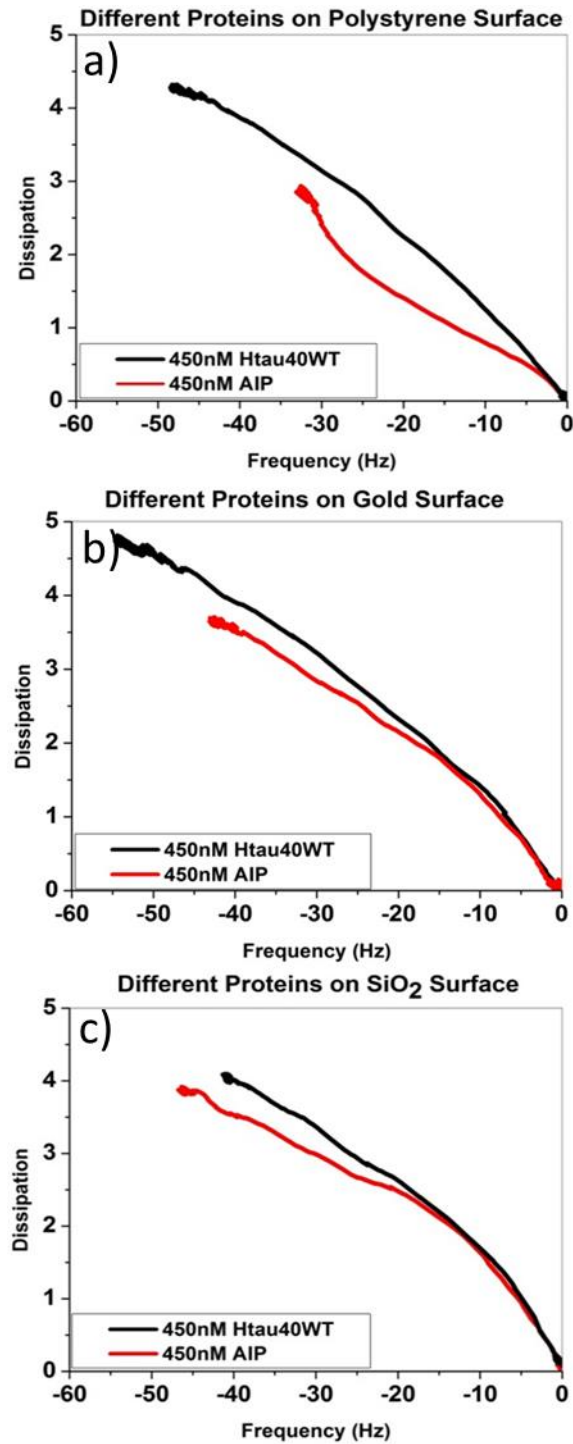


Figure 10: Dissipation vs. Frequency plots of 450nM Htau40WT (black) and AIP (red) proteins on different surfaces: (a) polystyrene, (b) gold, and (c) silicon dioxide, showing that polystyrene surfaces show a difference in rigidity of the proteins, while silicon dioxide and gold surfaces do not.

**Evidence of protein aggregation and possible oligomer formation at the different surfaces:** The propensity of the different surfaces to induce aggregation, by inducing the formation of oligomers, was monitored by using ThT, a fluorescence indicator that has been shown to adsorb to aggregated forms of proteins<sup>59</sup>. ThT was run across a surface already saturated with proteins. Figure 11(a,b,c) presents our results as plots of the frequency as a function time for the ThT experiments on the gold, polystyrene, and silicon dioxide surfaces, respectively, and Figure 11(d,e,f) are plots of the calculated adsorbed mass as a function of time for the same experiments on the same surfaces. The green lines in these plots represent ThT adsorption to a surface with no protein, the black lines represent ThT adsorption to a surface saturated in the wild-type protein, and the red lines represent ThT adsorption to a surface saturated in AIP. On all three surfaces, when the proteins were absent, the ThT did not adsorb and therefore no change in frequency was seen. Similarly the total mass adsorbed was found to be negligible. Fig. 11(a) shows that on the polystyrene surface saturated with the wild-type protein, an initial maximum frequency change of -88 Hz occurred within 2.5 minutes, before becoming stable at -72 Hz. However, when the ThT was run over the polystyrene surface saturated with AIP, a maximum frequency change of only -28 Hz was achieved in 2 minutes. Similarly Fig 11(d) showed that the mass of ThT that adsorbed to the WT Htau40 covered surface was more than three times (1750 ng/cm<sup>2</sup>) the mass of ThT that adsorbed to a polystyrene surface containing AIP (500 ng/cm<sup>2</sup>). Interestingly, the adsorption of ThT to the gold surface covered with the two different proteins were comparable to that of the hydrophobic polystyrene surfaces, even though the mass of WT tau protein adsorbed to gold was found to be significantly higher than the polystyrene surface. Such a dramatic decrease in frequency and increase in adsorbed mass of ThT suggests the possibility of the formation of more protein oligomers in case of the WT tau proteins. Further, our results also suggest a lack of difference in the gold and polystyrene surfaces in inducing aggregation.

For the ThT adsorption to a silicon dioxide surface saturated with the wild-type protein, a maximum frequency change of -86 Hz was reached within 2.5 minutes, before slowly increasing to a value of -72 Hz. When the surface was saturated with AIP, the ThT adsorption caused a maximum frequency change

of -101 Hz in 2.5 minutes before slowly increasing to a final value of -75 Hz. These results indicate that unlike the proteins on the polystyrene and gold surfaces, the difference in the hydrophobicity of the two proteins did not cause any difference in the possible formation of oligomers on the hydrophilic silicon dioxide surface. While this result may be counterintuitive, our results are in agreement with a recent Monte Carlo simulation study that showed that a weakly attracting surface can retard aggregation of proteins with a high propensity to aggregate, while the same surface can accelerate aggregation of proteins with a lower propensity to aggregate, possibly by providing more nucleation sites for aggregation<sup>60</sup>. The results presented here suggest that for the tau proteins, the silicon dioxide surface possibly allows more nucleation points for protein oligomer formation.

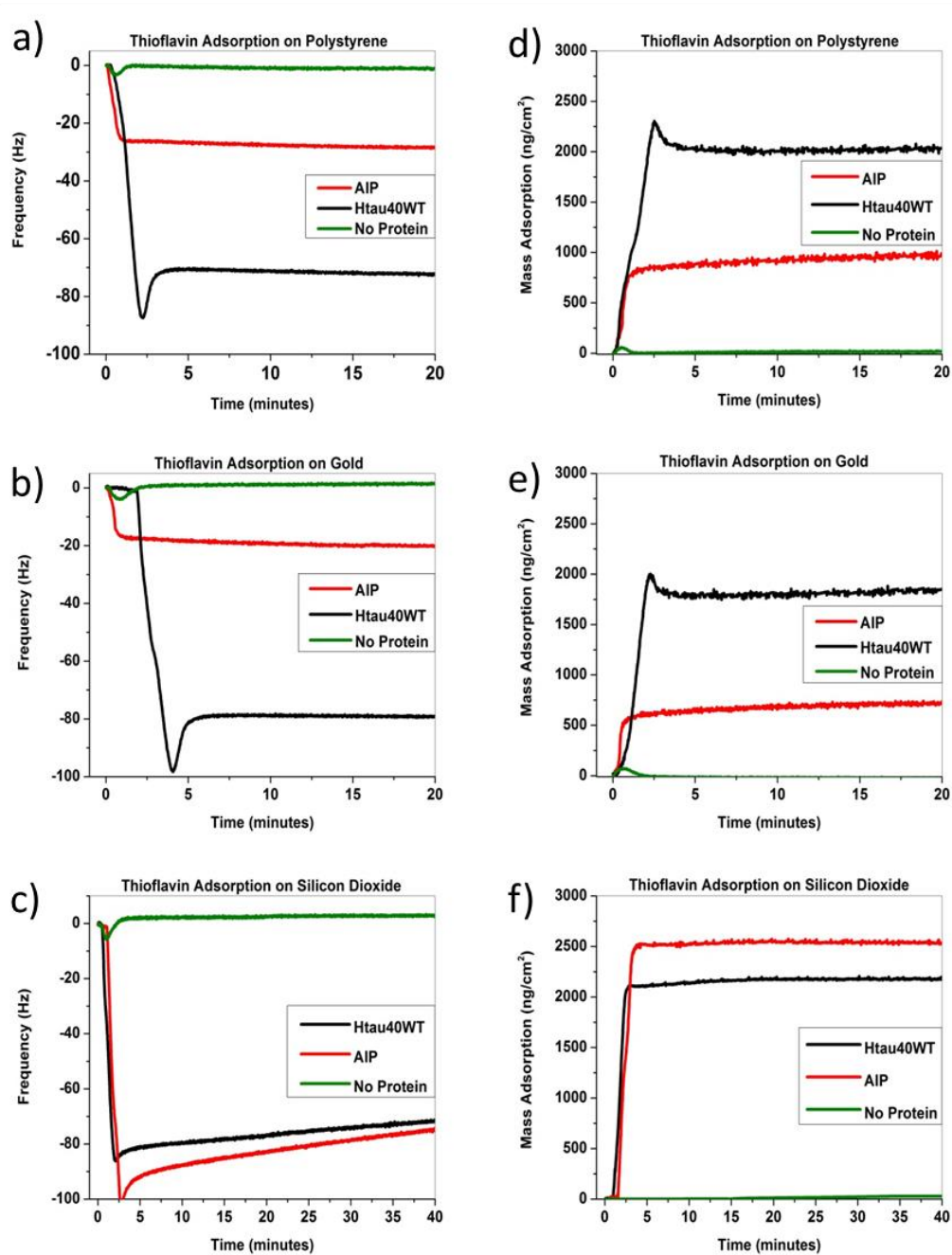


Figure 11: (a,b,c) change in frequency (Hz) and (d,e,f) change in the calculated adsorbed mass (ng/cm<sup>2</sup>) as a function of time, during the adsorption of the fluorescent indicator Thioflavin (ThT) to surfaces saturated with Htau40WT (black) or AIP (red) proteins, or a blank surface (green). ThT has been shown to adsorb to aggregated protein forms.

To further investigate the differences in surface induced aggregation of the WT Htau40 and AIP proteins, including possible oligomer formation, AFM images of the polystyrene and silicon dioxide surfaces was obtained, after incubation with 450 nM proteins for 20 hours. Fig. 12 provides representative

images of  $1\mu\text{m} \times 1\mu\text{m}$  sections of the surfaces, before and after protein adsorption. Fig. 12(a,d) are control polystyrene and silicon dioxide surfaces respectively and both of these surfaces show atomically flat surfaces. Incubation of the polystyrene surface (b, c) shows the formation of several aggregates (raised features) that are absent in case of AIP proteins. Only a few small aggregates were seen on the polystyrene surface in case of AIP. This direct imaging evidence also supports the ThT data shown in Fig. 11 where a significant difference was recorded between the two protein covered surfaces. As opposed to the polystyrene surface, the silicon dioxide surfaces showed several very large aggregates, when incubated with the WT proteins. Even though this number was not as high for AIP, the size of aggregates was higher than the polystyrene surfaces, further supporting our conclusion that the tendencies of the proteins to aggregate at the different surfaces is controlled by the intrinsic properties of the surfaces as well as the proteins. It must also be noted that at this nanomolar concentration none of the surfaces showed any fibril formation, even after five days of incubation. This is not surprising: Barrantes et al. showed that mica surfaces incubated with full length tau proteins at concentrations that were several orders of magnitude higher than the values reported here took up to eight months to show fibril formation<sup>61</sup>. Further, the QCM-D gold surfaces were atomically rough, such that differences between the surface morphology and protein aggregates could not be resolved.

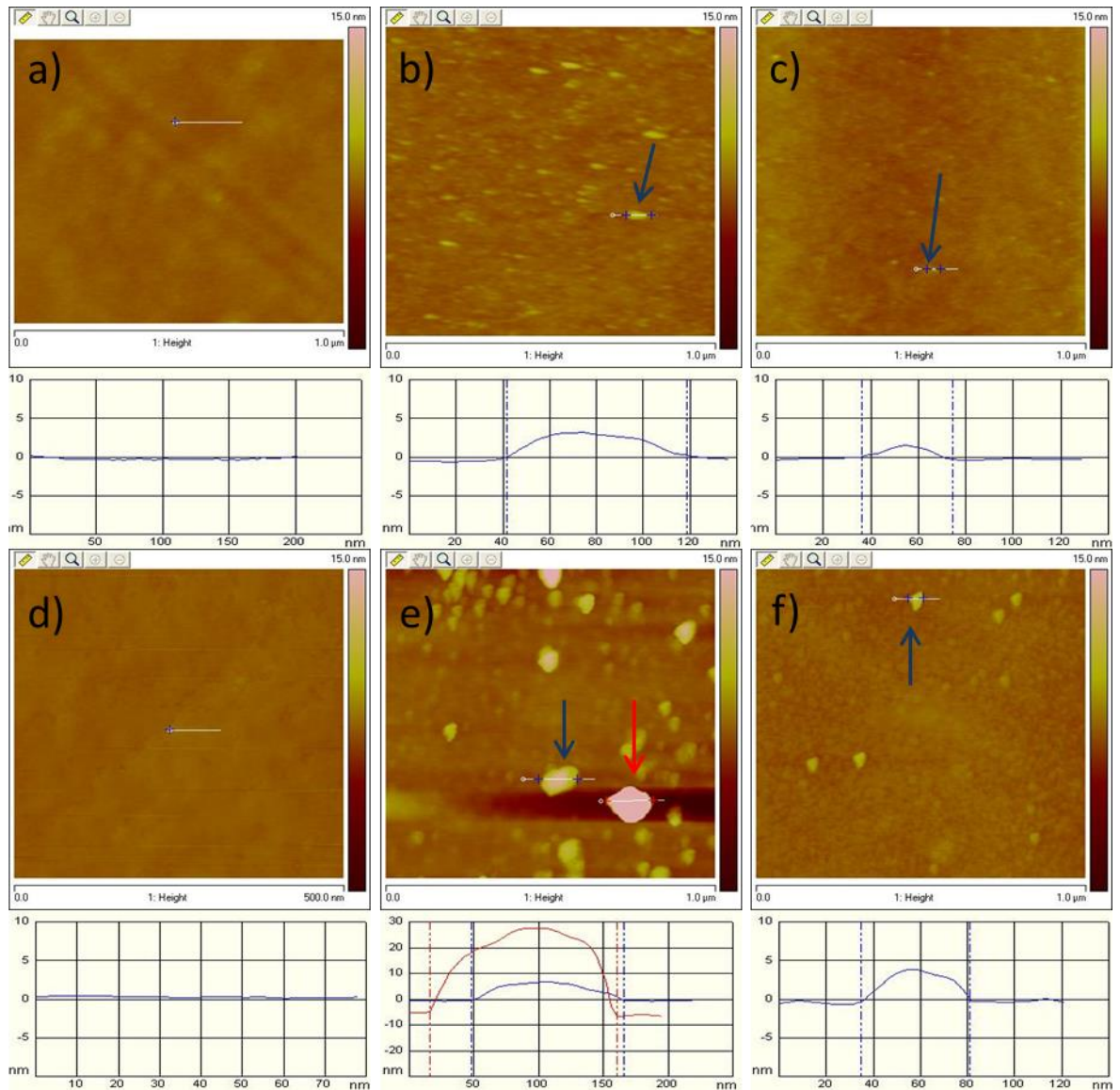


Figure 12: AFM images of wild-type tau protein and AIP on silicon dioxide wafers and polystyrene coated wafers. Image (a) and (d) show the bare polystyrene and silicon dioxide surfaces, respectively. These images show no surface features greater than 1nm high, which can be seen in the line graph below the image, and can therefore were considered flat. (b) shows the wild-type protein on the polystyrene surface, while (c) shows the AIP on polystyrene. (e) is an image of the wild-type tau protein on the silicon dioxide surface, while (f) is an image of the AIP on silicon dioxide, and there were few smaller aggregates present. The line graphs below each image represents the height of the surface features indicated by the arrows on the image themselves.

In summary, the observations presented here together confirm that adsorption of WT and AIP proteins is significantly modulated by hydrophobic properties of the surfaces, the nature of the proteins, as well as the strength of the binding of the proteins. Moreover, our results provided evidence suggesting that the charge of the surface has no noticeable effect on the adsorption of tau proteins. If there was an effect we would have seen an increase in the mass of protein adsorption to the negatively charged silicon dioxide



surface, when compared with the neutral gold surface, which showed the maximum adsorption. However, further experiments with different surface charges and charge densities are required to conclusively comment on the role of electrostatic interactions vs. hydrophobic and hydrophilic interactions in surface induced tau protein aggregation. Future experiments will also focus on other protein mutations, to further explore the effect of protein biochemistry on surface induced aggregation of tau proteins.

### **3.2 Adsorption and aggregation of proteins on lipid covered surfaces**

In this section I discuss the results of our research efforts focused on trying to model the interaction between the tau protein and a model cell membrane surface. To accomplish this, the QCM-D and AFM were again used together to allow us to gain access to data for both the adsorption and aggregation of tau on the lipid surface. Two lipid mixtures were used in these experiments: a 4:1 ratio of DPPE:DPPS and a 4:1 ratio of DPPE:DOPS. The two lipid head groups, PE and PS, were chosen because of their presence in the cells of the central nervous system, with PE lipids being one of the largest fraction of the phospholipids found in neurons<sup>33</sup>. When comparing the two mixtures, introducing DOPS in place of the DPPS adds an unsaturation in the tail group of the phospholipid, which is a very common strategy in biophysical studies to mimic the biphasic nature of cell membranes. A different mutation of tau was also used in these experiments: R5L. This protein has a mutation that occurs in its N-terminus; the part of the protein thought to be responsible for binding to the lipid membranes. Comparing this mutation to the wild-type tau protein would allow us to identify how significant the role of the N-terminus is in adsorbing to, aggregating, and possibly disrupting the cell membrane.

**Effect of Protein Biochemistry on Protein Adsorption to a Lipid Covered Surface:** The different lipid mixtures were run over the surface of a silicon dioxide wafer for 20 minutes and then the pump was turned off and the lipid solution was allowed to sit above the surface for about 20 more minutes. Figure 13 shows the change in the frequency of the sensor, when incubated with the lipid solution alone. From

this data it can be seen that the DPPE:DOPS mixture, which reached a maximum frequency change of -21 Hz, adsorbs slightly more than the DPPE:DPPS, which had a maximum frequency shift of around -16 Hz.

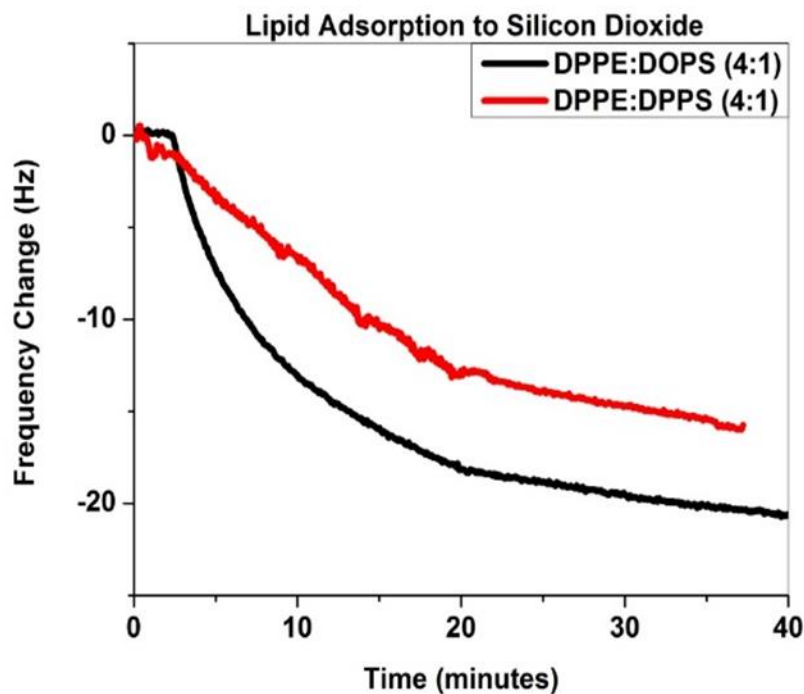


Figure 13: Lipid Adsorption to a silicon dioxide surface. Here we see that DPPE:DOPS adsorbs more than DPPE:DPPS, but more importantly, based on the shape of the curves for both lipid mixtures, we believe that the lipids adsorb as vesicles

Based on an analysis of the frequency and dissipation data during phospholipid adsorption, we conclude that these lipids adsorb as vesicles, and do not open up to form lipid bilayers on the surface. Vesicle to bilayer conversions have been studied extensively by various researchers<sup>62, 63</sup>. Piantavigna et al have used a QCM-D study to show that vesicle to bilayer transitions are accompanied by an increase in the frequency and decrease in dissipation over a long time to account for the entrapped fluid (buffer) that is released from the vesicles. After the frequency change reached a saturation value, the proteins of interest were run across the lipid coated sensors, to determine how they adsorbed to the lipid surface. For the first lipid mixture, DPPE:DPPS as shown in Figure 14, it was seen that the frequency change for the wild-type protein reached a maximum value around -45 Hz, where it then leveled off and remained for the remainder of the experiment. For R5L however, an interesting trend was seen. The frequency change for

this protein reached a maximum value of around -36 Hz, lower than the wild-type. However, long term incubation with the protein solution at 25 C resulted in a gradual increase in frequency, showing that the total mass of lipid and or protein adsorbed on the sensor was decreasing. We hypothesize that the increased hydrophobicity of the N-terminus in R5L has an increased ability to not only insert itself into the lipid membrane, but subsequently also cause disruption of the lipid vesicles by forming pores in the lipid membrane, which in turn could lead to loss of material from the surface. It has been shown that amyloid beta has the ability to form pore like oligomeric species of A $\beta$  upon interaction with the phospholipid membrane. Pore formation has been thought to induce cell death by disrupting membrane integrity and permeability<sup>64</sup>. We hypothesize that this same phenomenon may also be true for the early stage tau oligomers and we believe could be responsible for the shift in mass seen for the frequency change of R5L.

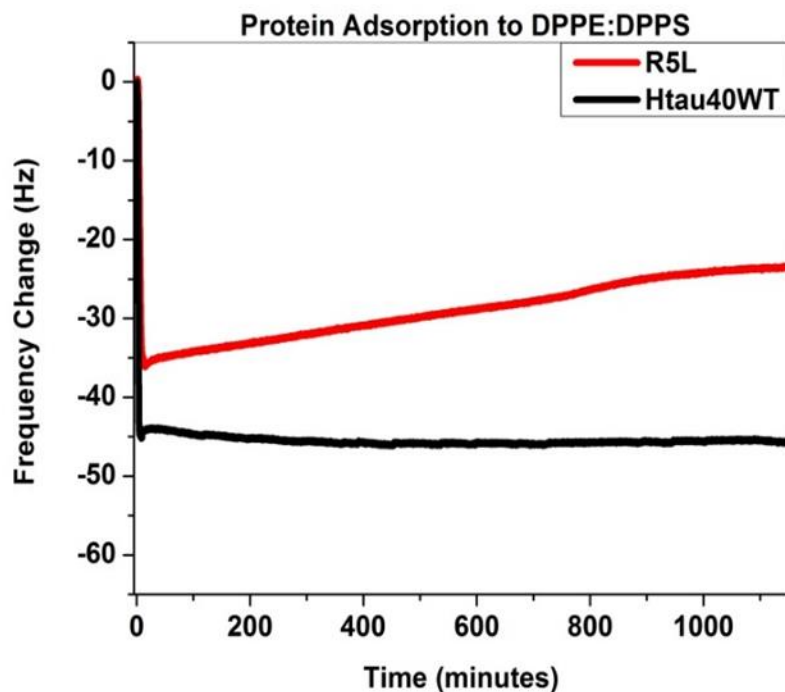


Figure 14: Different Proteins adsorption to a surface covered in DPPE:DPPS. Htau40WT (black) adsorbs more than R5L (red), but over time we see a loss of mass for the surface with R5L. This could possibly be due to the protein rupturing the lipid vesicle which then releases fluid and results in the mass decrease.

For the more fluid, DPPE:DOPS lipid mixture, as shown in Figure 15, the wild-type shows an initial frequency shift to a maximum of around -38 Hz before increasing to a final frequency shift of around -26 Hz. The trend discussed above for R5L is present for the wild-type for this lipid mixture proving that the wild-type protein also has the ability to disrupt the lipid membrane. However, ease of insertion of the proteins into the lipid membrane is possibly a first step in the pore formation process. Reaffirming what we saw for R5L above, the mutated tau protein's adsorption to this lipid mixture reached a maximum frequency shift of -55 Hz before a significant decrease in mass was seen as the frequency increased to -15 Hz, suggesting loss of vesicle integrity, possibly due to pore formation in the lipid membrane.

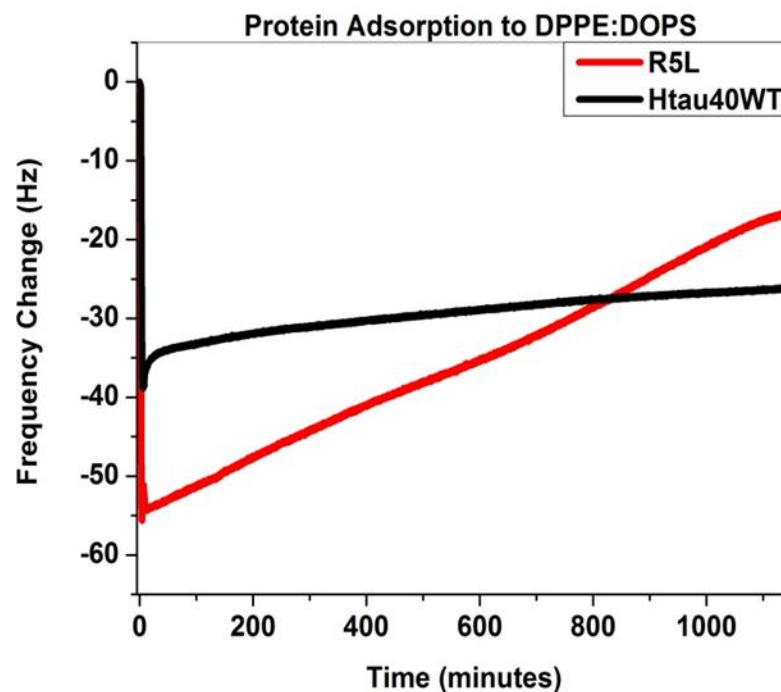


Figure 15: Different proteins adsorption to a surface covered in DPPE:DOPS. R5L (red) adsorbs more than Htau40WT (black), but over time there is a significant loss of mass for the surface with R5L. This is again most likely attributed to a disruption in the lipid vesicle. Interestingly, we see a similar trend, although not to the same extent, with the wild-type protein showing that it too has the ability to penetrate the lipid membrane.

**Effect of Lipid Composition on Protein Adsorption:** Next, we looked at the comparison between the same protein's adsorption on the different lipids to determine if the membrane characteristics could have an effect on the protein adsorption. The data presented previously was reorganized to allow a direct

comparison of each individual protein's adsorption to the different lipid surfaces. First, in Figure 16 we see adsorption of the wild-type proteins to both the DPPE:DPPS lipid mixture and the DPPE:DOPS lipid mixture. From this data we see that initially the wild-type adsorbs only slightly more to the DPPE:DPPS before the rise in the frequency seen in the data for the DPPE:DOPS created a much larger difference at the end of the experiment.

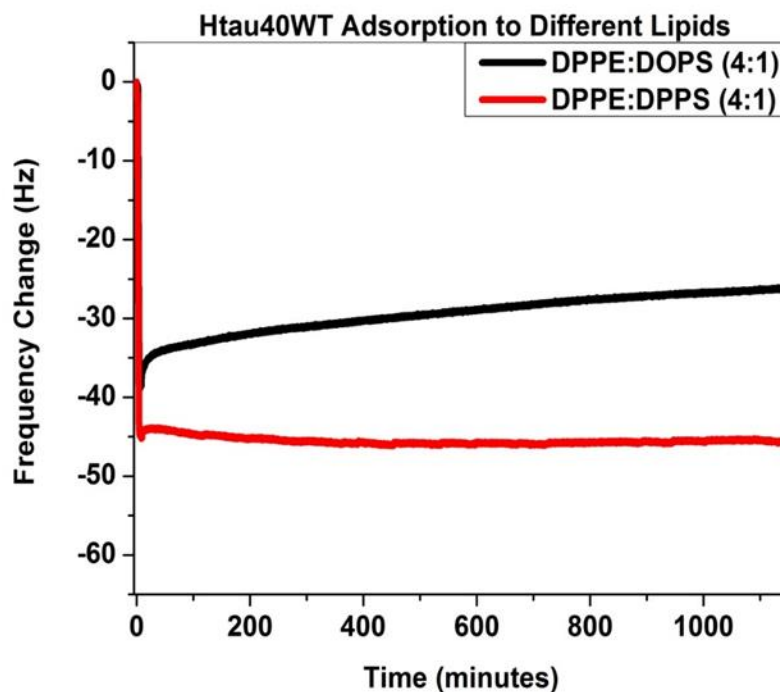


Figure 16: Adsorption of Htau40WT to a surface covered in DPPE:DPPS (red) and DPPE:DOPS (black). The wild-type protein adsorbs slightly more to the DPPE:DPPS surface, but for the surface covered in DPPE:DOPS, the wild-type protein seems to have the ability to rupture the vesicle, possibly due to the DPPE:DOPS being a more fluid mixture than the DPPE:DPPS.

For R5L, in Figure 17, initially we saw a much greater adsorption to the DPPE:DOPS surface. The trend of mass loss was then seen in both lipid experiments but the mass loss for the DPPE:DOPS was much greater. The presence of mass loss on the DPPE:DOPS for the wild-type protein, and the much larger mass loss for R5L on this surface, can be attributed to the unsaturation found in the DOPS. This characteristic, which is not found in the fully saturated DPPE:DPPS mixture, would make the membrane less rigid and allow for easier protein insertion and subsequent pore formation, accounting for our results.

This is important because in the cell membranes found in the human nervous system, there are unsaturations present, making them more susceptible to protein insertion, pore formation, and eventually cell death. Based solely on the data from the QCM-D, we could not definitively say that this pore formation was the cause of the mass loss. Therefore we employed the AFM to obtain high resolution images to visualize the mechanisms of protein interaction with the lipid surface.

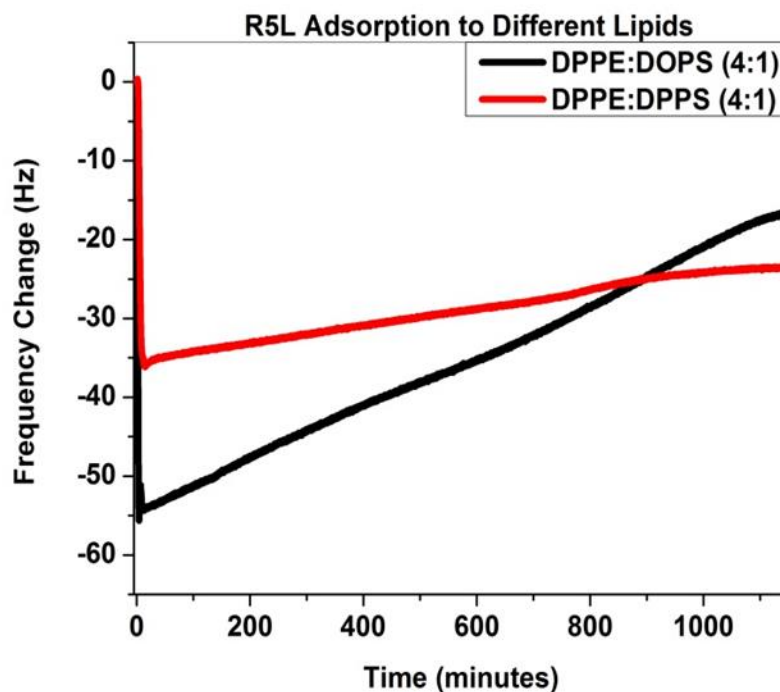


Figure 17: R5L adsorption to a surface covered in DPPE:DPPS (red) and DPPE:DOPS (black). The protein adsorbs more to the DPPE:DOPS surface and we see that R5L seems to have the ability to penetrate and rupture both lipids, but has the ability to do so to a greater extent in the more fluid DPPE:DOPS covered surface.

**AFM Visualization of Protein Adsorption to Lipid Surfaces:** The lipid mixtures were put onto the silicon dioxide wafers and then dried onto the surface at a high temperature in order to assure that they opened up and formed a bilayer on the surface. These wafers were then put into a protein solution of wild-type or R5L. One of the lipid bilayer containing wafers was also placed into a buffer solution without any proteins to serve as the control system. Figure 18 shows the results of the AFM images of the lipid covered interface after incubation with proteins. Figure 18a shows a silicon wafer with only the lipid

mixture. This image shows that the lipid mixture formed a uniform layer on the surface and would allow for the protein features to be more distinguishable. Figure 18b is an image of the wild-type protein on the lipid surface. We can see from this image the presence of a significant amount of protein aggregates. Further justifying the assumption that the wild-type protein can disrupt the lipid surface, a close examination of the images show circular pore-like formations, anywhere from 1nm to 3nm in height and around 40nm to 60nm in diameter, on the surface. In case of the R5L proteins on the lipid surface, shown in Figure 18c, we found several aggregates many of which appear to be pore-like structures. Figure 18d is a zoomed in image from the area in the red square in c, which has a large number of these pores. These findings further assert our QCM-D results and provide direct support of our hypothesis that tau proteins with hydrophobic mutations on the N-terminus induce pore formation in phospholipid membranes leading to a decrease in membrane integrity. Such pore formations are possibly the cause of cytotoxicity of Tau protein oligomers leading to the death of the neurons in the human brain.

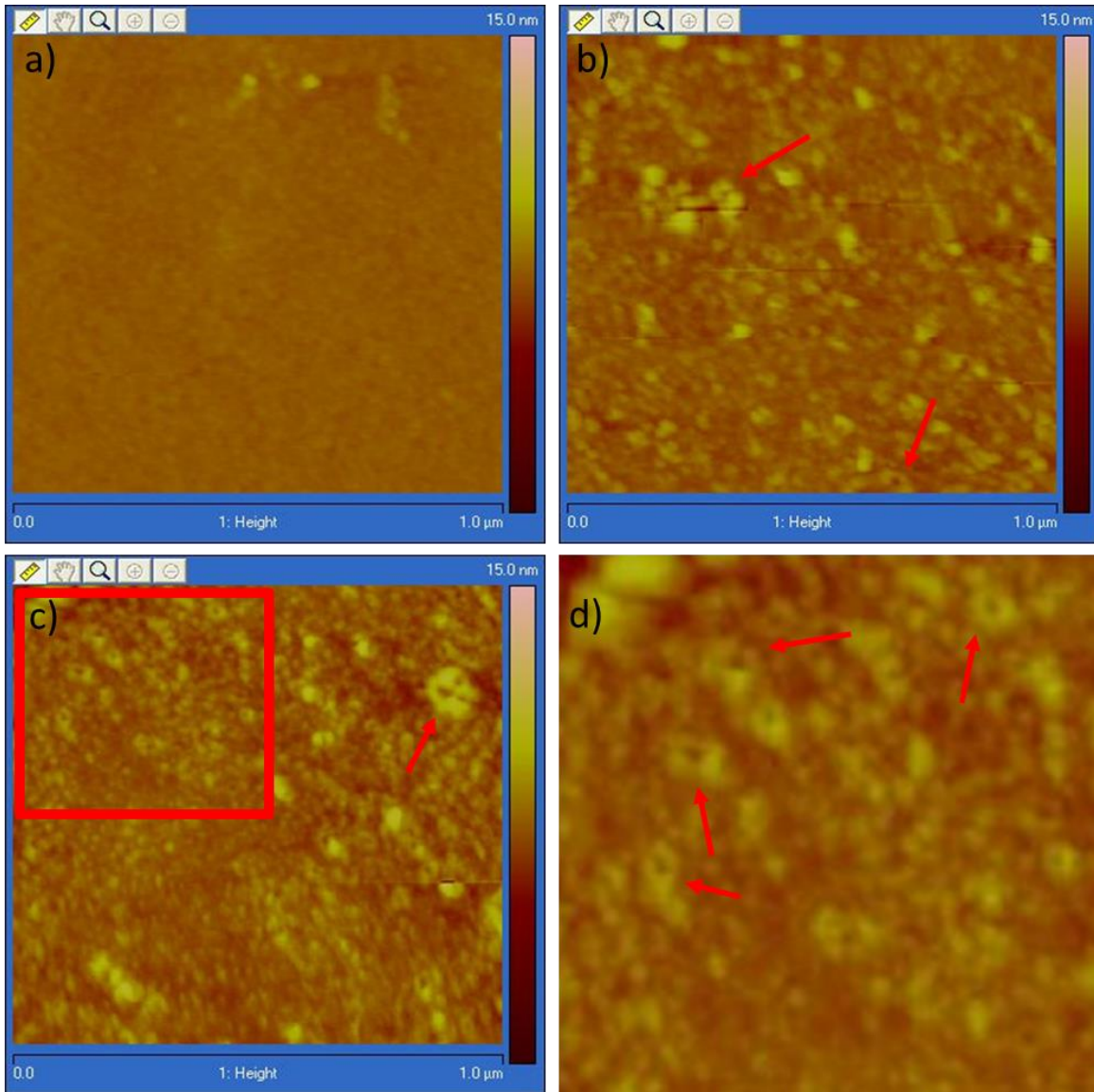


Figure 18: AFM images of (a) a surface with just DPPE:DOPS, (b) Htau40WT on a surface covered in DPPE:DOPS, (c) R5L on a surface covered in DPPE:DOPS, and (d) a zoomed in image of the red box on (c). We can see from (a) that the lipid forms a uniform layer on the surface. From (b) and (c) we can see that both proteins have the ability to form oligomers, and even more importantly, on both, although to a greater extent in the presence of R5L, there is the formation of what could be pores in the lipid surface.



## CHAPTER 4

### CONCLUSION AND FUTURE DIRECTION

In conclusion, the results presented for the experiments on bare surfaces show that adsorption of WT Htau40 and AIP proteins to hydrophobic and hydrophilic surfaces as well as surface-mediated aggregation of the tau proteins at these model surfaces is modulated by both the chemistry of the proteins as well as the surface chemistry. WT Htau 40 proteins showed increased adsorption and formation of small oligomeric species at the hydrophobic polystyrene surfaces when compared with AIP. Since the only difference between the WT protein and the AIP mutant lies in the differences in the MTBR, our results conclusively show that at hydrophobic surfaces, adsorption and aggregation of protein tau is due to the hydrophobicity of the microtubule binding regions of the proteins. This is also true for the gold surfaces. On the other hand, both WT and AIP proteins provided evidence of comparable adsorption and protein oligomer formation at the hydrophilic surfaces, although the amount of WT protein adsorbed to a hydrophilic surface was less than the adsorption to a hydrophobic surface. In fact, the hydrophilic surface was able to induce significant protein oligomer formation even in an assembly incompetent mutant. Our results together suggest that in addition to the biochemistry of the protein, the chemical properties of the surfaces modulate aggregation of Tau proteins at model surfaces.

The results of our experiments using lipid covered surfaces led us to the conclusion that both forms of tau have a strong affinity for binding to the lipid surface. Further, the significant decrease in mass seen in our QCM-D data, and formation of pores depicted in the AFM images indicate that while both proteins, have the ability to disrupt and rupture the lipid membrane by forming pores in the lipid surface, this effect is significantly enhanced in case of the R5L protein with a hydrophobic mutation at the N-terminus. Pore formation in oligomeric species leading to leakage of cells resulting in cell death is believed to be a major reason for protein toxicity in cells. However, to the best of our knowledge, this is the first direct evidence of lipid induced pore formation in full length tau protein aggregates.

The QCM-D coupled with the AFM allowed us to gain further insight into the mechanism of the tau protein adsorption and aggregation at solid surfaces, as well as at a model lipid membrane surface. The results of our experiments have given us confidence that our methods can, and will be used in the future to further investigate the tau protein's interaction with lipid membrane surfaces.

## CHAPTER 5

### SUMMARY

The adsorption and aggregation of an intrinsically disordered soluble protein, tau, into insoluble filaments is a defining hallmark of many neurodegenerative diseases, commonly referred to as tauopathies. When healthy, tau protein acts as a microtubule stabilizing protein, aiding in the structure and function of those microtubules. Aggregated variants of this protein, including neurofibrillary tangles and early stage oligomers, lead to cell death through either destabilization of microtubules, disruption of cell membranes, or some combination of both. Because of the detrimental outcomes of tauopathies, it is necessary to better understand the governing principles that modulate the initial steps in the mechanism of tau protein aggregation. The vast presence of surfaces such as the cell membrane in the macromolecular environment has been implicated as a possible inducer of the aggregation of tau. This role of surfaces, however, had not been explored in detail prior to this work. We hypothesized that Tau protein aggregation at model surfaces was modulated by two factors, the physicochemical properties of the surfaces, as well as the biochemistry of the protein molecules. We used two separate studies to justify our hypothesis: bare surfaces as a template of adsorption and aggregation, and lipid covered surfaces as a model cell membrane surface. We were able to show that on the bare surfaces, the slight hydrophobicity in the microtubule binding region of the wild-type tau protein allowed for more than a 25% increased adsorption to the hydrophobic surfaces over the mutant, A1P, which was missing this hydrophobicity. We saw more than 150% increase in Thioflavin adsorption to the wild-type protein over the A1P on the two hydrophobic surfaces, but a small difference on the silicon dioxide surface; both results were supported by AFM imaging. For the adsorption to lipid covered surface, we showed that both proteins, but primarily R5L, were able to rupture the lipid vesicles that were adsorbed to the surface. AFM imaging allowed us to visualize this interaction and also showed visual evidence of pore formation in the lipid membrane. This research project has given support in justifying our method for further research into the mechanism of tau aggregation.

## REFERENCES

1. Chiti, F.; Dobson, C. M. Protein misfolding, functional amyloid, and human disease. In *Annual Review of Biochemistry*, 2006; Vol. 75, pp 333-366.
2. Soto, C. Unfolding the role of protein misfolding in neurodegenerative diseases. *Nature Reviews Neuroscience* **2003**, *4* (1), 49-60.
3. Association, A. s. Basics of Alzheimer's Disease. (accessed 4/20/15).
4. Masters, C. L.; Simms, G.; Weinman, N. A.; Multhaup, G.; Mcdonald, B. L.; Beyreuther, K. Amyloid Plaque Core Protein in Alzheimer-Disease and down Syndrome. *P Natl Acad Sci USA* **1985**, *82* (12), 4245-4249.
5. Seeman, P.; Seeman, N. Alzheimer's Disease: beta-Amyloid Plaque Formation in Human Brain. *Synapse* **2011**, *65* (12), 1289-1297.
6. Aging, N. I. o. Alzheimer's Disease: Unraveling the Mystery. nia.nih.gov.
7. Gendron, T. F.; Petrucelli, L. The role of tau in neurodegeneration. *Molecular Neurodegeneration* **2009**, *4*.
8. Drubin, D. G.; Kirschner, M. W. TAU-PROTEIN FUNCTION IN LIVING CELLS. *Journal of Cell Biology* **1986**, *103* (6), 2739-2746.
9. Mohorko, N.; Bresjanac, M. TAU PROTEIN AND HUMAN TAUOPATHIES: AN OVERVIEW. *Zdravniški Vestnik-Slovenian Medical Journal* **2008**, *77*, II35-II41.
10. Luk, C.; Compta, Y.; Magdalinou, N.; Martí, M. J.; Hondhamuni, G.; Zetterberg, H.; Blennow, K.; Constantinescu, R.; Pijnenburg, Y.; Mollenhauer, B.; Trenkwalder, C.; Van Swieten, J.; Chiu, W. Z.; Borroni, B.; Cámara, A.; Cheshire, P.; Williams, D. R.; Lees, A. J.; de Silva, R. Development and assessment of sensitive immuno-PCR assays for the quantification of cerebrospinal fluid three- and four-repeat tau isoforms in tauopathies. *Journal of Neurochemistry* **2012**, *123* (3), 396-405.
11. Himmelstein, D. S.; Ward, S. M.; Lancia, J. K.; Patterson, K. R.; Binder, L. I. Tau as a therapeutic target in neurodegenerative disease. *Pharmacology & Therapeutics* **2012**, *136* (1), 8-22.
12. Maas, T.; Eidenmuller, J.; Brandt, R. Interaction of tau with the neural membrane cortex is regulated by phosphorylation at sites that are modified in paired helical filaments. *Journal of Biological Chemistry* **2000**, *275* (21), 15733-15740.
13. Snyder, S. W.; Lador, U. S.; Wade, W. S.; Wang, G. T.; Barrett, L. W.; Matayoshi, E. D.; Huffaker, H. J.; Krafft, G. A.; Holzman, T. F. AMYLOID-BETA AGGREGATION - SELECTIVE-INHIBITION OF AGGREGATION IN MIXTURES OF AMYLOID WITH DIFFERENT CHAIN LENGTHS. *Biophysical Journal* **1994**, *67* (3), 1216-1228.
14. Maguire-Zeiss, K. A. alpha-Synuclein: A therapeutic target for Parkinson's disease? *Pharmacological Research* **2008**, *58* (5-6), 271-280.
15. Ha, A. D.; Fung, V. S. C. Huntington's disease. *Current Opinion in Neurology* **2012**, *25* (4), 491-498.
16. Selkoe, D. J. Toward a comprehensive theory for Alzheimer's disease - Hypothesis: Alzheimer's disease is caused by the cerebral accumulation and cytotoxicity of amyloid beta-protein. *Ann Ny Acad Sci* **2000**, *924*, 17-25.
17. Hsiao, K.; Chapman, P.; Nilsen, S.; Eckman, C.; Harigaya, Y.; Younkin, S.; Yang, F. S.; Cole, G. Correlative memory deficits, A beta elevation, and amyloid plaques in transgenic mice. *Science* **1996**, *274* (5284), 99-102.
18. Geula, C.; Wu, C. K.; Saroff, D.; Lorenzo, A.; Yuan, M. L.; Yankner, B. A. Aging renders the brain vulnerable to amyloid beta-protein neurotoxicity. *Nature Medicine* **1998**, *4* (7), 827-831.
19. Nabeshima, T.; Itoh, A. Alzheimer's disease animal models induced by continuous infusion of beta-amyloid protein and anti-nerve growth factor antibody. *Reviews on Heteroatom Chemistry* **1997**, *16*, 229-255.
20. Boutajangout, A.; Wisniewski, T. Tau-Based Therapeutic Approaches for Alzheimer's Disease - A Mini-Review. *Gerontology* **2014**.

21. Castillo-Carranza, D. L.; Sengupta, U.; Guerrero-Munoz, M. J.; Lasagna-Reeves, C. A.; Gerson, J. E.; Singh, G.; Estes, D. M.; Barrett, A. D.; Dineley, K. T.; Jackson, G. R.; Kaye, R. Passive immunization with Tau oligomer monoclonal antibody reverses tauopathy phenotypes without affecting hyperphosphorylated neurofibrillary tangles. *J Neurosci* **2014**, *34* (12), 4260-72.
22. Haass, C.; Selkoe, D. J. Soluble protein oligomers in neurodegeneration: lessons from the Alzheimer's amyloid beta-peptide. *Nat Rev Mol Cell Biol* **2007**, *8* (2), 101-12.
23. Chi, E. Y.; Frey, S. L.; Winans, A.; Lam, K. L. H.; Kjaer, K.; Majewski, J.; Lee, K. Y. C. Amyloid-beta Fibrillogenesis Seeded by Interface-Induced Peptide Misfolding and Self-Assembly. *Biophysical Journal* **2010**, *98* (10), 2299-2308.
24. Kowalewski, T.; Holtzman, D. M. In situ atomic force microscopy study of Alzheimer's beta-amyloid peptide on different substrates: New insights into mechanism of beta-sheet formation. *P Natl Acad Sci USA* **1999**, *96* (7), 3688-3693.
25. Yu, Y. P.; Zhang, S.; Liu, Q.; Li, Y. M.; Wang, C.; Besenbacher, F.; Dong, M. D. 2D amyloid aggregation of human islet amyloid polypeptide at the solid-liquid interface. *Soft Matter* **2012**, *8* (5), 1616-1622.
26. Shen, L.; Adachi, T.; Vanden Bout, D.; Zhu, X. Y. A mobile precursor determines amyloid-beta peptide fibril formation at interfaces. *J Am Chem Soc* **2012**, *134* (34), 14172-8.
27. Giacomelli, C. E.; Norde, W. Conformational changes of the amyloid beta-peptide (1-40) adsorbed on solid surfaces. *Macromolecular Bioscience* **2005**, *5* (5), 401-407.
28. Saraiva, A. M.; Pereira, M. C.; Brezesinski, G. Is the Viscoelasticity of Alzheimer's A beta 42 Peptide Oligomers a General Property of Protein Oligomers Related to Their Toxicity? *Langmuir* **2010**, *26* (14), 12060-12067.
29. Kunze, G.; Barre, P.; Scheidt, H. A.; Thomas, L.; Eliezer, D.; Huster, D. Binding of the three-repeat domain of tau to phospholipid membranes induces an aggregated-like state of the protein. *Biochimica Et Biophysica Acta-Biomembranes* **2012**, *1818* (9), 2302-2313.
30. Elbaum-Garfinkle, S.; Ramlall, T.; Rhoades, E. The Role of the Lipid Bilayer in Tau Aggregation. *Biophysical Journal* **2010**, *98* (11), 2722-2730.
31. Barre, P.; Eliezer, D. Structural transitions in tau k18 on micelle binding suggest a hierarchy in the efficacy of individual microtubule-binding repeats in filament nucleation. *Protein Science* **2013**, *22* (8), 1037-1048.
32. Jones, E. M.; Dubey, M.; Camp, P. J.; Vernon, B. C.; Biernat, J.; Mandelkow, E.; Majewski, J.; Chi, E. Y. Interaction of Tau Protein with Model Lipid Membranes Induces Tau Structural Compaction and Membrane Disruption. *Biochemistry* **2012**, *51* (12), 2539-2550.
33. Wells, K.; Farooqui, A.; Liss, L.; Horrocks, L. Neural membrane phospholipids in alzheimer disease. *Neurochem Res* **1995**, *20* (11), 1329-1333.
34. Cleveland, D. W.; Hwo, S. Y.; Kirschner, M. W. Purification of tau, a microtubule-associated protein that induces assembly of microtubules from purified tubulin. *J Mol Biol* **1977**, *116* (2), 207-25.
35. Cleveland, D. W.; Hwo, S. Y.; Kirschner, M. W. Physical and chemical properties of purified tau factor and the role of tau in microtubule assembly. *J Mol Biol* **1977**, *116* (2), 227-47.
36. Binder, L. I.; Frankfurter, A.; Rebhun, L. I. The distribution of tau in the mammalian central nervous system. *J Cell Biol* **1985**, *101* (4), 1371-8.
37. Weingarten, M. D.; Lockwood, A. H.; Hwo, S. Y.; Kirschner, M. W. A protein factor essential for microtubule assembly. *Proc Natl Acad Sci U S A* **1975**, *72* (5), 1858-62.
38. Ballatore, C.; Lee, V. M.; Trojanowski, J. Q. Tau-mediated neurodegeneration in Alzheimer's disease and related disorders. *Nat Rev Neurosci* **2007**, *8* (9), 663-72.
39. Buee, L.; Bussiere, T.; Buee-Scherrer, V.; Delacourte, A.; Hof, P. R. Tau protein isoforms, phosphorylation and role in neurodegenerative disorders. *Brain Res Brain Res Rev* **2000**, *33* (1), 95-130.
40. Delacourte, A.; Buee, L. Tau pathology: a marker of neurodegenerative disorders. *Curr Opin Neurol* **2000**, *13* (4), 371-6.
41. Carlson, S. W.; Branden, M.; Voss, K.; Sun, Q.; Rankin, C. A.; Gamblin, T. C. A complex mechanism for inducer mediated tau polymerization. *Biochemistry* **2007**, *46* (30), 8838-49.

42. Wischik, C. M.; Novak, M.; Edwards, P. C.; Klug, A.; Tichelaar, W.; Crowther, R. A. Structural characterization of the core of the paired helical filament of Alzheimer disease. *Proc Natl Acad Sci U S A* **1988**, *85* (13), 4884-8.
43. von Bergen, M.; Barghorn, S.; Muller, S. A.; Pickhardt, M.; Biernat, J.; Mandelkow, E. M.; Davies, P.; Aebi, U.; Mandelkow, E. The core of tau-paired helical filaments studied by scanning transmission electron microscopy and limited proteolysis. *Biochemistry* **2006**, *45* (20), 6446-57.
44. Chang, E.; Kim, S.; Yin, H.; Nagaraja, H. N.; Kuret, J. Pathogenic missense MAPT mutations differentially modulate tau aggregation propensity at nucleation and extension steps. *Journal of Neurochemistry* **2008**, *107* (4), 1113-1123.
45. Gasteiger E., H. C., Gattiker A., Duvaud S., Wilkins M.R., Appel R.D., Bairoch A. Protein Identification and Analysis Tools on the ExPASy Server. In *The Proteomics Protocols Handbook*, Walker, J. M., Ed.; Humana Press, 2005, pp 571-607.
46. Chirita, C. N.; Necula, M.; Kuret, J. Anionic Micelles and Vesicles Induce Tau Fibrillization in Vitro. *Journal of Biological Chemistry* **2003**, *278* (28), 25644-25650.
47. Mohsen, R.; Thorne, J. B.; Alexander, B. D.; Snowden, M. J. Deposition of fluorescent NIPAM-based nanoparticles on solid surfaces: Quantitative analysis and the factors affecting it. *Colloids and Surfaces A: Physicochemical and Engineering Aspects* **2014**, *457* (0), 107-115.
48. Stange, T. G.; Mathew, R.; Evans, D. F.; Hendrickson, W. A. SCANNING TUNNELING MICROSCOPY AND ATOMIC FORCE MICROSCOPY CHARACTERIZATION OF POLYSTYRENE SPIN-COATED ONTO SILICON SURFACES. *Langmuir* **1992**, *8* (3), 920-926.
49. Carmel, G.; Mager, E. M.; Binder, L. I.; Kuret, J. The structural basis of monoclonal antibody Alz50's selectivity for Alzheimer's disease pathology. *Journal of Biological Chemistry* **1996**, *271* (51), 32789-32795.
50. Necula, M.; Kuret, J. A static laser light scattering assay for surfactant-induced tau fibrillization. *Analytical Biochemistry* **2004**, *333* (2), 205-215.
51. Rankin, C. A.; Sun, Q.; Gamblin, T. C. Pseudo-phosphorylation of tau at Ser202 and Thr205 affects tau filament formation. *Molecular Brain Research* **2005**, *138* (1), 84-93.
52. Al Abdulal, E.; Khot, A.; Bailey, A.; Mehan, M.; Debies, T.; Takacs, G. A. Surface characterization of polystyrene treated with ozone and grafted with poly(acrylic acid). *Journal of Adhesion Science and Technology* **2015**, *29* (1), 1-11.
53. Voinova, M. V.; Jonson, M.; Kasemo, B. Dynamics of viscous amphiphilic films supported by elastic solid substrates. *J Phys-Condens Mat* **1997**, *9* (37), 7799-7808.
54. Rodahl, M.; Hook, F.; Fredriksson, C.; Keller, C. A.; Krozer, A.; Brzezinski, P.; Voinova, M.; Kasemo, B. Simultaneous frequency and dissipation factor QCM measurements of biomolecular adsorption and cell adhesion. *Faraday Discuss* **1997**, *107*, 229-246.
55. Ozansoy, M.; Basak, A. N. Tauopathies: A distinct class of neurodegenerative diseases. *Balkan Journal of Medical Genetics* **2007**, *10* (2), 3-14.
56. Lin, X. H.; Liao, G. L.; Tang, Z. R.; Shi, T. L. UV surface exposure for low temperature hydrophilic silicon direct bonding. *Microsystem Technologies-Micro-and Nanosystems-Information Storage and Processing Systems* **2009**, *15* (2), 317-321.
57. Jeganathan, S.; von Bergen, M.; Mandelkow, E.-M.; Mandelkow, E. The Natively Unfolded Character of Tau and Its Aggregation to Alzheimer-like Paired Helical Filaments†. *Biochemistry* **2008**, *47* (40), 10526-10539.
58. Saraiva, A. M.; Cardoso, I.; Saraiva, M. J.; Tauer, K.; Pereira, M. C.; Coelho, M. A. N.; Mohwald, H.; Brzezinski, G. Randomization of Amyloid-beta-Peptide(1-42) Conformation by Sulfonated and Sulfated Nanoparticles Reduces Aggregation and Cytotoxicity. *Macromolecular Bioscience* **2010**, *10* (10), 1152-1163.
59. Biancalana, M.; Koide, S. Molecular mechanism of Thioflavin-T binding to amyloid fibrils. *Biochimica Et Biophysica Acta-Proteins and Proteomics* **2010**, *1804* (7), 1405-1412.
60. Vacha, R.; Frenkel, D. Relation between Molecular Shape and the Morphology of Self-Assembling Aggregates: A Simulation Study. *Biophysical Journal* **2011**, *101* (6), 1432-1439.

61. Barrantes, A.; Sotres, J.; Hernando-Perez, M.; Benitez, M. J.; de Pablo, P. J.; Baro, A. M.; Avila, J.; Jimenez, J. S. Tau aggregation followed by atomic force microscopy and surface plasmon resonance, and single molecule tau-tau interaction probed by atomic force spectroscopy. *J Alzheimers Dis* **2009**, *18* (1), 141-51.
62. Mechler, A.; Praporski, S.; Piantavigna, S.; Heaton, S. M.; Hall, K. N.; Aguilar, M.-I.; Martin, L. L. Structure and homogeneity of pseudo-physiological phospholipid bilayers and their deposition characteristics on carboxylic acid terminated self-assembled monolayers. *Biomaterials* **2009**, *30* (4), 682-689.
63. Piantavigna, S.; McCubbin, G. A.; Boehnke, S.; Graham, B.; Spiccia, L.; Martin, L. L. A mechanistic investigation of cell-penetrating Tat peptides with supported lipid membranes. *Biochimica et Biophysica Acta (BBA) - Biomembranes* **2011**, *1808* (7), 1811-1817.
64. Lasagna-Reeves, C. A.; Sengupta, U.; Castillo-Carranza, D.; Gerson, J. E.; Guerrero-Munoz, M.; Troncoso, J. C.; Jackson, G. R.; Kaye, R. The formation of tau pore-like structures is prevalent and cell specific: possible implications for the disease phenotypes. *Acta neuropathologica communications* **2014**, *2*, 56.